UNIVERSITY OF
CAMBRIDGE

Numerical Studies of Shock-Induced Ignition

Jeffrey Salmond, *Darwin College*

August 2012

This dissertation is submitted for the degree of Master of Philosophy.

Declaration

I hereby declare that this dissertation is the result of my own work and includes nothing which is the outcome of work done in collaboration except where specifically indicated in the text. In addition, this dissertation is approximately 11420 words in length.

Acknowledgements

I would like to thank my supervisor Dr Nikos Nikiforakis for his guidance and encouragement. Thanks are also due to the other members of the Laboratory for Scientific Computing especially: Stefan Schoch, Louisa Michael and Elise Croft for many helpful discussions.

I also would like to thank my sponsors Dr Caroline Handley and Dr Andrew Barlow at AWE for their enthusiasm and direction. I also gratefully acknowledge the financial support of AWE.

Summary

In this study, numerical solutions of 1-D piston impact problems have been obtained for the evolution from shock induced ignition to steady state detonation of two different high-explosives, Nitromethane (NM) and LX-17.

I have designed and written a numerical model (hydrocode). This is based on a finite volume solution of the augmented Euler equations for the mixture of reactants and products. These are solved with equations of state defined for the mixture, and with a reaction rate law. The hydrocode was designed to investigate different options for equations of state for reactants and products, with several different closure conditions and different reaction laws. The components of hydrocode were validated by comparison with other published results and excellent agreement was obtained.

For NM the use of a *single* JWL equation of state fitted to the mixture of reactants and products was compared with a *combined* equation of state (derived from two separate JWL equations of state for the reactant and the product phases with a closure condition of temperature equilibrium). The best comparison with experimental results was obtained with the combined approach. One of the main contributions of this thesis is to focus on the ignition phase of the NM cases. Excellent agreement with recent experiments of Dattelbaum [11] have been obtained through careful empirical selection of parameters - we believe this is the first comparison with the ignition phase of the process.

For LX-17, a combined equation of state obtained from a pair of JWL equations for reactants and products was investigated with three different closure conditions: (i) temperature equilibrium, (ii) constant volume ratio and (iii) isentropic. For each of the closure conditions two different reaction models (i) ignition and growth and (ii) a simple reaction rate law were tested. It has been found that the three closure conditions produce broadly similar results. The constant volume ratio, which is the cheapest computationally, being as good as the widely used temperature equilibrium or the more complex isentropic condition - suggesting that the constant volume ratio closure condition is a good candidate for extension to more complex situations. Although others have concentrated on comparisons for the final steady state of the process, we have also presented a comparison of the closure conditions for the ignition phase.

Contents

List of Figures

List of Tables

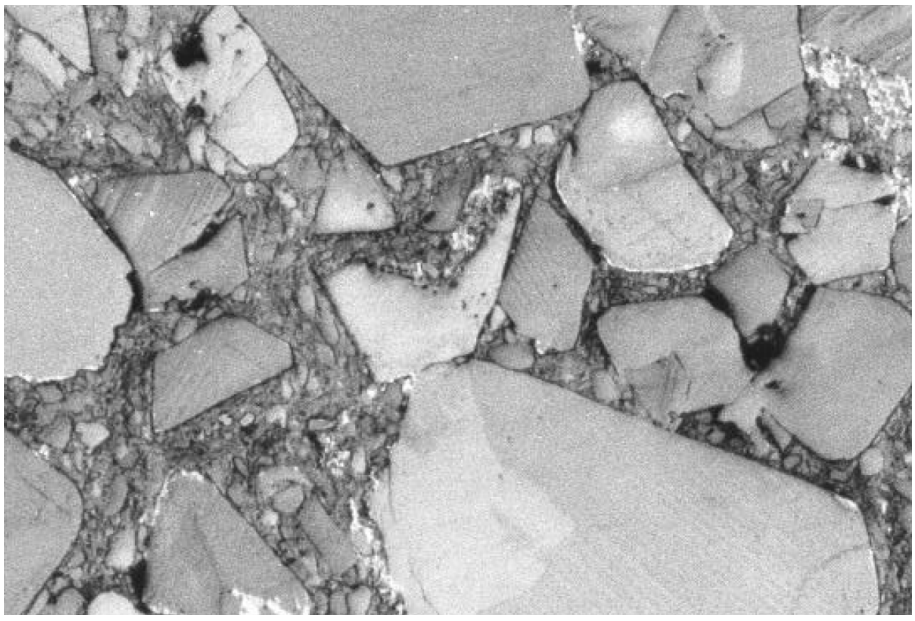

Figure 1: Scanning electron microscope image showing the microstructure of explosive PBX-9501. Magnification is such that the width of the area shown is $1mm$.

1. Introduction

This thesis reports the first phase of a project on numerically modelling the shock to detonation transition in explosives with complex microstructure. The project is sponsored by AWE.

The mathematical modelling of shock induced detonation in high explosive materials is a challenging problem that has attracted a substantial research effort for many years. In a high explosive, a shock or some other external stimulus can cause the formation of a detonation wave. This is a self sustaining shock which provides energy to the material causing it to react. The wave is then reinforced by the energy released by the reaction. The form of the detonation wave itself is well understood through the theoretical work originally by Chapman and Jouguet, and extended by Zel'dovich, von Neumann and Döring [15]. However, the processes involved in the formation of the detonation wave from the initial stimulus, particularly in complex materials, are still not well understood.

In order to correctly model these effects it is essential that the numerical solver should accurately generate the speed and shape of the input shock wave and the resulting detonation wave. For example, erroneous numerical overshoots in the shock capturing scheme may lead to early ignition. In this study, we have carefully checked that the numerical solver gives good results in this respect.

Two high-explosive materials are modelled in this project: (i) liquid Nitromethane and (ii) the manufactured polymer bonded explosive LX-17. Both of these materials exhibit complex micro-scale processes which make accurate numerical modelling difficult. In Nitromethane, this can be caused by artificially introduced impurities and turbulence in the fluid [11]. In LX-17 it stems from the heterogeneous micro-structure of crystalline fragments of the reactive compound and the plastic binder. Whilst the plastic binder is not itself energetically reactive, it does have an important role in the response of the explosive material. In particular, the shock compression of gas bubbles trapped in the binder material and adiabatic shear in the crystals of explosive play an important role. Figure 1 shows the crystalline structure of a typical polymer bonded explosive PBX-9501 [18].

This complexity leads to unintuitive results. The pure explosive itself responds quite predictably to external stimuli, with a clear energy threshold for ignition. However, the actual explosive material can be detonated by stimuli below this threshold [7]. This is attributed to the formation of *hotspots*, where the microscopic mechanical processes mentioned above can cause the temperature within a small region to be much higher than the average in the material. The reaction is initiated at these hotspots and then spreads into the bulk of the material, which leads to the formation of the detonation wave.

In both materials the length scale of these processes is much less than the scale of the hydrodynamics of the fluid and the numerical grid scale that is used to model these macroscopic processes. Therefore, to include these effects in hydrocodes, sub-grid-scale modelling and parameterisation is needed.

1.1. Approach

Our approach builds on recent work by Handley [18] and others at AWE to model shock ignition and detonation propagation in high explosives using the augmented Euler equations. These equations describe the evolution of the mixture of explosive reactants and products. The equations are solved in the Eulerian frame, rather than the Lagrangian method of Handley [18] and others. A full discussion of the relative advantages of Eulerian and Lagrangian methods is given by Barlow [4, §1.1]. In order to apply the system of equations to particular materials, it is necessary to specify equations of state. This can be a single equation fitted to the mixture, or an equation of state implicitly defined by combining separate equations for each phase. In the latter case extra assumptions are needed to close the system.

We have performed numerical simulations of 1-D piston impact problems using a modelling framework (a hydrocode) which was developed to facilitate a range of numerical experiments. This framework consists of a state of the art hyperbolic solver [38] which addresses the inert part of the problem, and a well established ODE solver [28] for the source term (the reaction part of the problem). These are then coupled via Strang splitting [23]. These aspects of the numerical solution are described in §3.

One of the main purposes of this hydrocode is to allow comparison of the different approaches for forming the equation of state for the mixture. For the single equation of state formulation, evaluation is fairly straight-forward. However, for an implicit mixture of equations of state with appropriate closure condition, the root of a system of equations has to be found. This system can be badly behaved due to steep gradients and discontinuities and so the root finding procedure is the most computationally demanding part of the whole numerical solution: considerable effort has been taken in this study to develop an efficient and stable scheme.

In order to model the microscopic, sub-grid scale processes in the shock induced ignition of these complex materials, the ignition and growth model is used. This model, originally by Lee and Tarver [22] does not directly model the mechanisms that cause hotspots, but the effects are included by fitting a complex reaction rate to experimental results. This approach has been successfully applied by many researchers: for example by Banks [3], Kapila [20], Menikoff [24], Tarver [35, 36, 37], Whitworth [39].

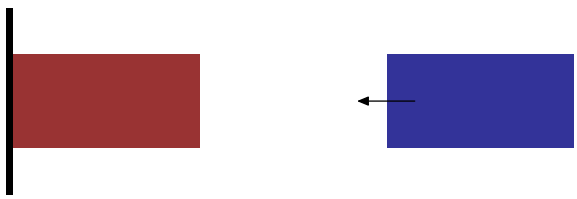

Figure 2: Sketch of a gas-gun experiment. The sample of explosive material (red) is stationary against a fixed wall and the flyer (blue) impacts from the right.

1.2. Overview of Numerical Experiments

Using the above approach, numerical solutions have been obtained for a number of versions of the piston impact problem. This is a 1-dimensional representation of a gas-gun experiment where the explosive sample is impacted by a high speed projectile which initiates a shock in the sample. This type of experiment is sketched in figure 2. Examples of experiments of this type and the results produced can be seen in the work of Gustavsen and Sheffield et al. [17, 32] and Dattelbaum et al. [11]. In the experiments performed by Campbell et al., the incoming shock is generated by a small explosive charge rather than a plate impact [7, 8].

For convenience, in the Eulerian numerical simulation we view the experiment in the frame of the impacting plate projectile. This is equivalent to simulating the explosive sample hitting a stationary wall.

Two different materials have been studied: Nitromethane and LX-17. For Nitromethane the mixture is composed of two components: the liquid nitromethane reactant and the product gases (H_2, N_2, H_2O and CO). This can be modelled using a single equation of state for both the liquid and gas phases or with separate equations of state for the liquid phase and the mixture of product gases. For LX-17 the mixture is composed of four components. The reactants: crystalline triaminotrinitrobenzene (TATB) explosive and solid polymer binder, and the products: gases resulting from the explosive reaction and vaporised binder. These four components were modelled using two separate equations of state for the reactants and the products.

The simulations were designed to capture both the ignition phase of the experiments and the evolution to the final state. These numerical experiments may be divided into three categories:

- Tests to validate the numerical solvers that can be compared with other published numerical and experimental results (see §A).
- Nitromethane experiments to determine the effect of having a single equation of state or an implicit mixture model (see §4).
- LX-17 experiments to determine the effect of using different closure conditions for the mixture model formulation (see §5).

Three different closure conditions were tested for LX-17 (i) the temperature equilibrium assumption which has been widely used by other workers for this type of problem, (ii) a constant volume approximation which was chosen to facilitate the numerical solution of the two equations of state, and (iii) an isentropic assumption, which is considered the most physically realistic of the three. This latter condition was motivated by the comments from Petitpas [27] on the shortcomings of the temperature closure (see below).

The need for a better understanding of the effects of these closure assumptions has been mentioned by other workers: see Handley [18, §3.1.3] and Whitworth [39, §2.4]. Stewart [34] has compared the three closure conditions for a steady state solution, but we

present comparisons for the full evolution from shock to detonation which have not been previously obtained. This is one of the main contributions of this study.

A summary of the numerical experiments is contained in the following table:

Material	EOS Type	Figure Nos
Nitromethane	Single	10
	Mixture (Temperature)	11
LX-17	Mixture (Temperature)	17, 18, 23 & 24
	Mixture (Constant volume ratio)	19, 20, 25 & 26
	Mixture (Isentropic)	21, 22, 27 & 28

Numerical experiments have so far been confined to 1-dimensional problems with two states. This provides a strong foundation for proceeding to 2- and 3-dimensional problems with possibly three or more states. The structure of the numerical framework has been carefully designed to allow such future extensions. In particular, the solver of the equation of state can be used in multiple dimensions without modification.

1.3. Overview of Previous Work

In this brief overview, we separately discuss the three main elements of the hydrocode solution, namely: (i) modelling of the dynamics of the mixture, (ii) equations of state and closure conditions and (iii) the reaction rate law.

Modelling of Dynamics

There is a long history of modelling shock waves in an inert, compressible single fluid. The dynamics of an inviscid inert fluid are described by the Euler equations.

To model the flow of two interacting fluids, there have been several approaches. Baer and Nunziato (BN) [2] have axiomatically derived a seven equation model with separate treatment of each material. This model is accurate but very difficult to implement. It is rarely used with complex equations of state and has not been successfully extended to more than two reacting materials. This has been simplified to six and five equation models by Kapila, Bdzil, Menikoff et al. [5, 19] and other researchers: for example Saurel, Petitpas and coworkers [9, 26, 27, 29], and Allaire [1].

A second approach is to formulate a mixture model where the two materials are treated using one set of variables: density, momentum, energy and species concentration. The advantages of this mixture scheme are its simplicity and the fact that it can be extended to three or more materials. However, this formulation requires an additional assumption (a closure condition) which is not needed in the BN or five and six equation models (see for example Schwendeman [31]). As already indicated, this is the approach followed in this study.

Equations of State and Closure Conditions

A key element of this study is the investigation of equations of state and different closure conditions. The equation of state used is the Jones-Wilkins-Lee (JWL) equation [21].

When forming the mixture equation of state from the separate constituent equations of state, it is necessary to make an assumption about the energy exchange between the phases. The standard assumption is that the two phases are in temperature equilibrium. This is also seen in the work of Handley [18], Kapila and Schwendeman [20, 31] and most other researchers in this field.

Peptitas [27] has described some problems with assuming temperature equilibrium in this type of model. He concludes that temperature equilibrium is unphysical, as the timescale for this to be reached is several orders of magnitude longer than the timescales of the reaction. In this thesis, we shall experiment with different closure conditions and quantify the effect of these various assumptions. Stewart [33] compares temperature to isentropic closure for steady state calculations. We extend this work to proper time evolution from ignition to steady state.

Reaction Rate Law

To evolve λ - the volume fraction of unreacted explosive to products - the pressure dependent *ignition and growth* model of Lee and Tarver [22] has been used in the simulations by Kapila [20] and others. The model is based on the assumption that ignition starts at hot spots and grows outwards which is supported by experimental observations.

Another reaction rate model found in the literature is the Arrhenius temperature dependent rate law used by Handley [18] and others which enables more direct modelling of the physics of the reaction.

1.4. Structure of Thesis

The mathematical model is presented in §2. This consists of the augmented Euler equations for the mixture, the equations of state with closure conditions and the reaction model.

The numerical method is discussed in §3. This describes the finite volume hyperbolic solver and an ODE solver for the source term.

In §4 and §5, piston impact experiments are presented to test the different formulations. These numerical simulations closely mirror the experimental setup used in gas-gun experiments, which makes validation against experimental results possible. As a starting point for the numerical experiments in §5, the one dimensional simulations performed by Kapila [20] have been repeated. This allows parts of the code to verified against independent results as shown in appendix A.

2. Mathematical Models

To model the dynamics of a reacting fluid, we shall use the time-dependant Euler equations for an inert fluid and augment them to include a model of the reaction. The Euler equations are introduced in §2.1 and the extension to a mixture of reactive fluids is presented in §2.2. To complete the mathematical model of the reacting materials, the equations of state used in this work are described in §2.3 and the relevant reaction rate laws are presented in §2.4.

2.1. Euler Equations

The Euler equations quantify the conservation of mass, momentum and energy for high speed gas dynamics. For a (single) homogeneous, compressible and inviscid fluid in one space dimension the Euler equations can be written in conservation form:

$$\frac{\partial}{\partial t}\mathbf{Q} + \frac{\partial}{\partial x}\mathbf{F}(\mathbf{Q}) = 0 \tag{1}$$

where the vector of conserved variables and the flux function are defined as:

$$\mathbf{Q} = \begin{pmatrix} \rho \\ \rho u \\ \rho E \end{pmatrix} \qquad \mathbf{F}(\mathbf{Q}) = \begin{pmatrix} \rho u \\ \rho u^2 + p \\ u(\rho E + p) \end{pmatrix} \tag{2}$$

where ρ, u and p are the *primitive* variables corresponding to density, velocity and pressure. The total energy per unit mass E is defined as the sum of the kinetic energy and the internal energy:

$$E = \left(\frac{1}{2}u^2 + e\right) \tag{3}$$

where e is the specific internal energy. To close the system, we require a definition of e as a function of the primitive variables. This is referred to as a *caloric* equation of state. In §2.3, some of the more common equations of state are presented.

If the Euler equations are augmented by other physical effects, namely the effects of viscosity and heat conduction, we recover the Navier-Stokes equations [38]. These terms are safely neglected in this work as the processes that we are modelling occur over very short timescales - the typical length of the simulations performed in this report is 10^{-6} s.

However, in some other works involving high speed reacting flows [16], these terms were found to have an important contribution. In particular, including the effects of heat conduction and turbulence could be could be important to model the physical processes that cause hotspots in a complex material. A full discussion of the relevant physics that is included and omitted is found in Handley [18, §2.1].

The extension to a mixture of reacting fluids is described below as an augmentation of the Euler equations. This extension could be applied identically to the full Navier-Stokes formulation.

2.2. Reactive Mixture Models

To fully describe two fluids moving in total disequilibrium, the axiomatic model of Baer and Nunziato [2] (BN) can be regarded as the most general formulation as it uses a full set of Euler equations for each phase and sophisticated source terms to describe the exchange of mass and energy between the phases. This requires $3N + (N - 1)$ conservation equations for N phases. However, this model is extremely complicated and (to my knowledge) has not been successfully applied to more than two reacting materials.

To simplify the BN model to a more tractable system, a different paradigm is applied. Instead of modeling the different phases of the fluid directly, we choose to model a homogeneous mixture of the constituent fluids. The fluids are assumed to be in mechanical equilibrium, having equal pressure and moving with the same velocity - this has been termed a *Mixture Model*.

The validity of these assumptions is discussed in a series of papers by Bdzil, Kapila et al. [5, 19]. They conclude that in the very fast physical process of detonation, pressure and velocity relaxation occurs on very short timescales and non-equilibrium effects can be safely neglected. A qualitative assessment of the differences between solutions produced by the BN and mixture models is presented by Schwendeman et al. [31].

As result of these assumptions, the mixture model requires only $3 + (N - 1)$ equations for N phases and may be written in conservation form:

$$\frac{\partial}{\partial t}\mathbf{Q} + \frac{\partial}{\partial x}\mathbf{F}(\mathbf{Q}) = \mathbf{S}(\mathbf{Q}) \tag{4}$$

with the conserved variables, flux function and reactive source term given (for two phases):

$$\mathbf{Q} = \begin{pmatrix} \rho \\ \rho u \\ \rho E \\ \rho\lambda \end{pmatrix} \qquad \mathbf{F}(\mathbf{Q}) = \begin{pmatrix} \rho u \\ \rho u^2 + p \\ u(\rho E + p) \\ \rho u \lambda \end{pmatrix} \qquad \mathbf{S}(\mathbf{Q}) = \begin{pmatrix} 0 \\ 0 \\ 0 \\ \rho\mathcal{R} \end{pmatrix} \tag{5}$$

Here, the primitive variables ρ, u, p define the specific density, velocity and pressure of the mixture of fluids. E is the total energy per unit mass and $\mathcal{R}$ is a reaction rate. The new variable λ quantifies the progress of the reaction. Some common forms for the reaction rate are given in §2.4. As before, E is the sum of the internal and kinetic energies for the mixture of fluids, as in (3). Now, e is the specific internal energy for the mixture of fluids which is defined by a mixture equation of state which takes the form $e = e\,(\rho,\, p,\, \lambda)$. The different methods of forming this mixture equation of state are investigated in §4 and §5.

In this project, we are interested only in application to a mixture of two fluids, although this methodology can be used to model a mixture of an arbitrary number of fluids [16]. However, extending to more than three fluids with complex equations of state quickly becomes very computationally demanding [3].

2.3. Equations of State

In order to close the systems of conservation laws used in section §4 and §5, an equation of state is defined. By careful design of the equation and its parameters, the conservation laws can be applied to specific materials. The *caloric* equation relates pressure (p) and specific volume (v) to internal energy (e), and the *thermal* equation is used to calculate the temperature (T):

$$e = e(v, p) \qquad T = T(v, p) \tag{6}$$

The caloric and thermal equations are closely related and both are necessary for a complete hydrodynamic description of a material. Whilst the temperature does not appear explicitly in the Euler equations, it is needed for the mixture laws in §5.

Other quantities can be derived from these equations. In order to calculate optimal sizes for the timestep used in the solver (see §3.4), the sound speed (a) is used. This is given by:

$$a = \sqrt{\frac{v^2\left(p + \frac{\partial e}{\partial v}\right)}{\frac{\partial e}{\partial p}}} \tag{7}$$

For most equations of state, this formula can be derived analytically, but it is sometimes more convenient to calculate a numerical estimate.

In this work, two different equations of state are used. The simplest is the Ideal Gas equation defined by equation (8). For the materials under investigation is §4 and §5 however, the Jones-Wilkins-Lee equation defined by (10) and (11) is used.

These are not the only options, and other forms for the equation of state that are frequently encountered in the literature are the Williamsburg [6, 14] and Linear Grüneisen [18] equations. It would be straightforward to apply the numerical approach of this study to these alternatives.

Ideal Gas

The ideal gas or polytropic equation of state is suitable for most real gases at room temperatures and pressures. The equations of state are:

$$e = \frac{pv}{\gamma - 1} \qquad T = \frac{pv}{C_v(\gamma - 1)} \tag{8}$$

where γ is the (constant) adiabatic index and C_v is the heat capacity. The speed of sound is easily derived using the relation (7):

$$a = \sqrt{\frac{\gamma p}{\rho}} \tag{9}$$

In this study, the ideal gas equations are only used for code verification in §A.1, where they are used to simulate air in Toro's inert shock tube tests. The parameters used for air are $\gamma = 1.4$ and $C_v = 0.718\ \left[\frac{\text{kJ}}{\text{kg K}}\right]$.

Jones-Wilkins-Lee

To simulate the real explosive materials Nitromethane and LX-17, the Jones-Wilkins-Lee (JWL) [21] equations of state are used. In §4 and §5, JWL equations are prescribed for both the reactants and products. For the reactants, the parameters for the equation of state are found by fitting to experimental shock compression data. For the products, the parameters are fitted to the results of cylinder detonation tests and other metal acceleration data [21, 36, 37].

The caloric and thermal equations of state are given:

$$e(v,p) = \frac{pv}{\omega} - F(v) + F(v_0) + Q \tag{10}$$

$$T(v,p) = \frac{1}{C_v}\left(\frac{pv}{\omega} - Z(v) + Z(v_0)\right) \tag{11}$$

where the auxiliary functions $F(v)$ and $Z(v)$ are defined by:

$$F(v) = A\left(\frac{v}{\omega} - \frac{1}{R_1}\right)e^{-R_1 v} + B\left(\frac{v}{\omega} - \frac{1}{R_2}\right)e^{-R_2 v} \tag{12}$$

$$Z(v) = A\left(\frac{v}{\omega}\right)e^{-R_1 v} + B\left(\frac{v}{\omega}\right)e^{-R_2 v} \tag{13}$$

Here A, B, R_1 and R_2 are the fitted parameters. Q is the heat released by this phase, C_v is the heat capacity and ω is the Grüneisen coefficient, related to the adiabatic index by $\omega = \gamma - 1$.

If $A = B = 0$, the JWL formulation reduces to the ideal gas equation given above.

JWL is commonly used in explosive calculations (see for example: Tarver [22, 36, 35, 37] and Kapila and coworkers [3, 20, 30]) and so it has a very reliable parameter set. In particular, it is often used in combination with the ignition and growth reaction rate described in §2.4 to describe the type of non-heterogeneous crystalline explosives under investigation in this project.

The Nitromethane experiments in §4 use the parameter set from Tarver and Urtiew [37] which are chosen to match the experiments by Sheffield et al. [32]. The LX-17 experiments in §5 use a parameter set originally by Gustavsen et al. [17] and further investigated by Tarver [36], and Kapila and coworkers [20]. The parameters for both materials are given in table 1.

2.4. Reaction Rates

This section describes the reaction rate modelling used in this project. These rate laws are used to define the source term in equation (4).

$$\mathbf{S}(\mathbf{Q}) = \Big(0,\, 0,\, 0,\, \rho\mathcal{R}(\mathbf{Q})\Big) \tag{14}$$

Ignition and Growth

The ignition and growth rate law (originally by Lee and Tarver [22]) is a phenomenological [25] attempt to make a macro-scale description of microscopic effects such as hotspots. The model is based on the assumption that ignition starts at hot spots and grows outwards. This is supported by experimental data. The reaction rate has three steps and can be written:

$$\mathcal{R} = \begin{cases} \mathcal{R}_I & \text{for } \lambda < \lambda_{ig} \\ \mathcal{R}_{G1} & \text{for } \lambda_{ig} < \lambda < \lambda_{G1} \\ \mathcal{R}_{G1} + \mathcal{R}_{G2} & \text{for } \lambda_{G2} < \lambda \end{cases} \tag{15}$$

where the three terms describe three stages of the reaction, and λ_{ig}, λ_{G1} and λ_{G2} are the volume fractions at which the three terms are activated. $\mathcal{R}_I$ models the hotspot formation, where a small fraction of the explosive is ignited which causes local pressure spikes. $\mathcal{R}_{G1}$ is a growth term describing the spread of hotspots into the bulk of the explosive and finally $\mathcal{R}_{G2}$ models the later times of the reaction when much of the explosive is burnt and the hotspots are coalescing.

The three terms are defined by:

$$\mathcal{R}_I = \mathcal{I}\,(1-\lambda)^b\,(\rho - 1 - a)^x \tag{16}$$

$$\mathcal{R}_{G1} = \mathcal{G}_1\,(1-\lambda)^c\,\lambda^d p^y \tag{17}$$

$$\mathcal{R}_{G2} = \mathcal{G}_2\,(1-\lambda)^e\,\lambda^g p^z \tag{18}$$

where a, b, c, d, e, g, x, y, z, $\mathcal{I}$, $\mathcal{G}_1$ and $\mathcal{G}_2$ are the constants that parameterise the model. These constants are defined experimentally. A common criticism of the ignition and growth model is that it cannot be predictive due to the large number of parameters that have to be matched to very specific experimental scenarios. A thorough discussion is found in Whitworth [39].

For the experiments on nitromethane in §4, a parameter set defined by Tarver and Urtiew [37] is used. For the experiments on LX-17 in §5, we use the parameter set defined by Gustavsen et al. [17] and further investigated by Tarver [36], and Kapila and coworkers [20]. The parameters for both materials are given in table 2.

By applying Chapman-Jouguet theory [15], we can find a form for the steady state detonation wave, and plot the reaction rate for this waveform. A plot for the nitromethane solution is shown in figure 3 and the corresponding plot for LX-17 in figure 4. Note how the rate varies over several orders of magnitude. This indicates that care should be taken when integrating the reactive source term.

	LX-17		Nitromethane	
	Reactants	Products	Reactants	Products
A [Pa]	778.1×10^{11}	14.8105×10^{11}	3×10^{12}	2.029×10^{11}
B [Pa]	-0.05031×10^{11}	0.6379×10^{11}	-1.8003×10^{9}	5.689×10^{9}
ω	0.8938	0.5	1.237	0.3
C_v [Pa/K]	2.487×10^{6}	1×10^{6}	1.4272×10^{6}	1.0×10^{6}
v_0 [m^3/kg]	1/1905	∞	1/1137	∞
Q [Pa − cc/cc]	6.9×10^{9}	0.0	5.7987×10^{9}	0.0
R_1	11.3	6.2	10	4.4
R_2	1.13	2.2	1.0	1.2

Table 1: Parameters for the Jones-Wilkins-Lee equation of state. Values for LX-17 taken from Gustavsen et al. [17] and values for nitromethane taken from Tarver & Urtiew [37].

LX-17

a	0.22	d	1.0	x	7	$\mathcal{I}$ [s^{-1}]	4×10^{12}	λ_{ig}	0.02
b	0.667	e	0.667	y	3	$\mathcal{G}_1$ [$(10^{11}\,\mathrm{Pa})^{-y}\,s^{-1}$]	4.5×10^{9}	λ_{G1}	0.8
c	0.667	g	0.667	z	1	$\mathcal{G}_2$ [$(10^{11}\,\mathrm{Pa})^{-z}\,s^{-1}$]	3×10^{7}	λ_{G2}	0.8

Nitromethane

a	0.5741	d	0.667	x	4	$\mathcal{I}$ [s^{-1}]	10^{9}	λ_{ig}	0.01
b	0.667	e	0.667	y	4	$\mathcal{G}_1$ [$(10^{11}\,\mathrm{Pa})^{-y}\,s^{-1}$]	1.21875×10^{11}	λ_{G1}	0.8
c	0.667	g	0.667	z	1	$\mathcal{G}_2$ [$(10^{11}\,\mathrm{Pa})^{-z}\,s^{-1}$]	2.4×10^{8}	λ_{G2}	0.8

Table 2: Parameters for the Ignition and growth reaction rate. Values for LX-17 taken from Gustavsen et al. [17] and values for nitromethane taken from Tarver & Urtiew [37].

LX-17

σ [s^{-1}]	5.5×10^{12}	ν	0.667	μ	1.0	n	3.25	λ_0	0.2

Table 3: Parameters for the simplified pressure dependant reaction rate.

Simple Pressure Dependant Rate Law

For some simulations of LX-17 in §5, a simplified rate law is proposed. This allows the simulations to be run without the complications introduced by the ignition and growth reaction rate. Similar to the form of the pressure dependant reaction rate given in Fickett [15], a function was devised that would imitate the growth term of the ignition and growth rate law in equation (17):

$$\mathcal{R} = \sigma\,(1-\lambda)^{\nu}\,(\lambda+\lambda_0)^{\mu}\,p^{n} \tag{19}$$

where σ, ν, μ, n and λ_0 are adjustable parameters. The parameters were chosen to provide a realistic detonation wave form without attempting to match any particular material. These parameters are given in table 3.

The reaction rate is plotted for a CJ solution in Figure 4 alongside ignition and growth for comparison. Pressure dependant rate laws are commonly used as pressure is a quantity that is easy to measure in experiments. This can, in some cases, make it easier to fit the rate law to measured experimental data.

2.5. Scaling

To minimise the errors in the solution caused by the finite precision computer arithmetic, it is useful to apply a scaling to the variables in the system so that calculations are performed on values with order of magnitude near one. Also, normalizing the time and length scales means that it is easy to predict the time taken for the explosive to ignite and the speed at which the detonation wave travels, which simplifies the design of the computational domain.

In the simulations of piston impact problems presented in §4 and §5, we choose to non-dimensionalise with respect to: (i) the initial density of the material ρ_0, (ii) the speed of the steady-state detonation wave D_{CJ} and (iii) a representative timescale t_{ref}. With these three quantities, we can define reference volume, pressure and length scales:

$$v_{\mathrm{ref}} = 1/\rho_0 \qquad p_{\mathrm{ref}} = D_{\mathrm{CJ}}^2/v_{\mathrm{ref}} \qquad l_{\mathrm{ref}} = D_{\mathrm{CJ}}\,t_{\mathrm{ref}} \tag{20}$$

which is sufficient to apply the scaling to all of the simulation parameters. The scaling constants for the two materials studied in this project are given in table 4, and all of the results presented are given in these scaled units.

	ρ_0 [kg/m^3]	D_{CJ} [m/s]	t_{ref} [s]
Nitromethane	1137	6243.2	10^{-6}
LX-17	1905	7679.9	10^{-6}

Table 4: Scaling constants.

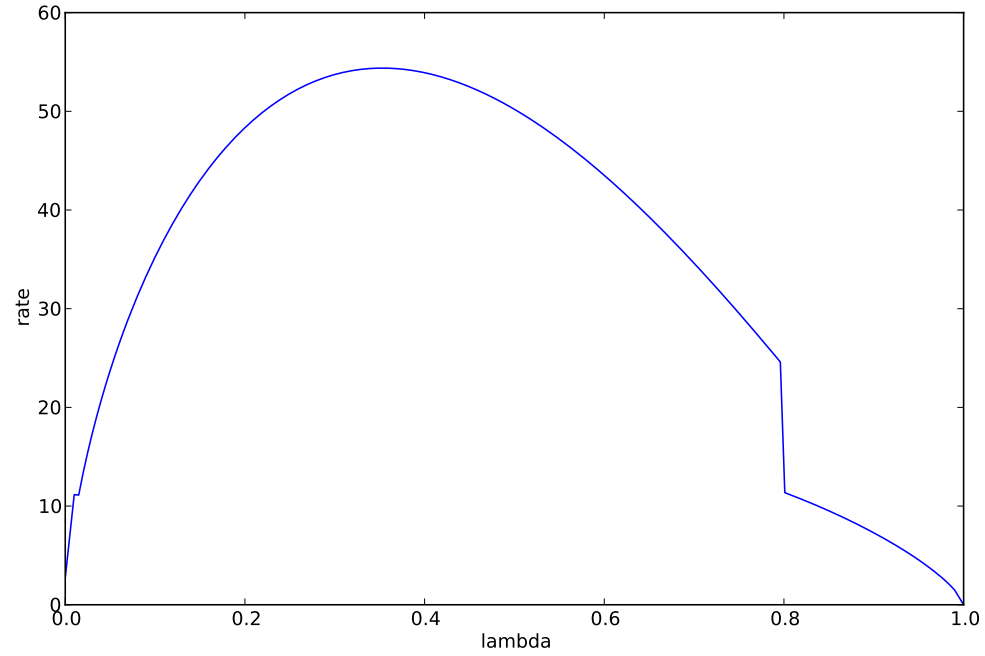

Figure 3: Plot of the ignition and growth reaction rate for nitromethane in a steady CJ state.

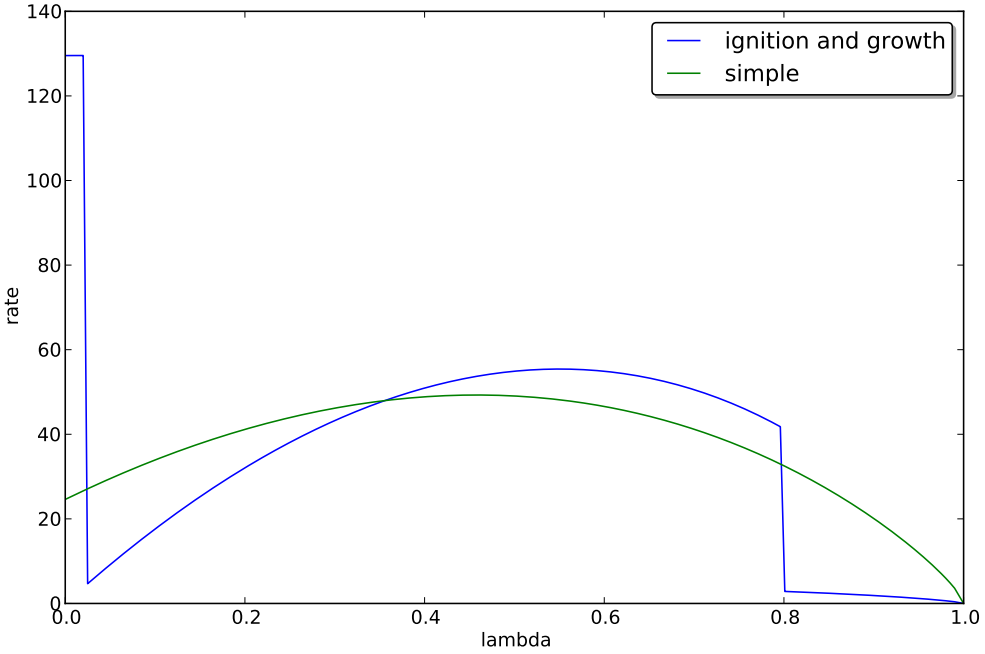

Figure 4: Plot of the reaction rates for LX-17 in a steady CJ state. The ignition and growth rate is shown in blue and my simplified rate in green.

3. Numerical Methods

To model the dynamics of the reacting mixture of fluids, the augmented Euler equations, as introduced in §2.2, will be used. The equations take the form:

$$\frac{\partial}{\partial t}\mathbf{Q} + \frac{\partial}{\partial x}\mathbf{F}(\mathbf{Q}) = \mathbf{S}(\mathbf{Q}) \tag{21}$$

where $\mathbf{Q}$ is the vector of the conserved variables, $\mathbf{F}(\mathbf{Q})$ is a flux function and $\mathbf{S}(\mathbf{Q})$ is the reactive source term. To solve equation (21), an operator splitting approach is used to divide the problem into the hyperbolic equations of fluid motion and a parabolic equation for the source term:

$$\frac{\partial}{\partial t}\mathbf{Q} + \frac{\partial}{\partial x}\mathbf{F}(\mathbf{Q}) = 0 \tag{22}$$

$$\frac{\partial}{\partial t}\mathbf{Q} = \mathbf{S}(\mathbf{Q}) \tag{23}$$

The splitting method is described in §3.1. The solvers for the hyperbolic component and for the source term are discussed in §3.2 and §3.5 respectively.

These methods are used to propagate the system from some known initial conditions at time t^0 to a later time t^N. Variable time steps are taken to move forward in time from t^n to t^{n+1}, until the required output time is attained. To minimise numerical errors, it is preferable to take as few timesteps as possible. The Courant-Friedrichs-Lewy (CFL) condition as described in §3.4 is used to calculate the largest possible timestep for which the hyperbolic solver is stable.

The final component of the numerical method is the boundary conditions at each end of the domain. For the simulations in §4 and §5, reflective and transmissive boundaries are required. These are described in §3.3.

3.1. Operator Splitting

The second order accurate Strang splitting approach [38, Chap. 15] is used to solve the inhomogeneous equation (21) by separately applying well known methods for the hydrodynamic system (22) and the reactive source term (23).

The complete scheme can be defined by operators $\mathcal{A}(\tau)$ and $\mathcal{B}(\tau)$ that numerically advance the solution by a time τ for the hydrodynamic and reactive parts of the system respectively. These operators are applied to advance the solution from Q^n at t^n to Q^{n+1} at t^{n+1}:

$$Q^{n+1} = \mathcal{B}\left(\Delta t^n/2\right)\ \mathcal{A}\left(\Delta t^n\right)\ \mathcal{B}\left(\Delta t^n/2\right) \tag{24}$$

This is a fractional step scheme that models the motion of the inert fluid mixture by operator $\mathcal{A}$ and the reaction of a stationary fluid by operator $\mathcal{B}$. We advance by taking a half timestep in $\mathcal{B}$, a full timestep in $\mathcal{A}$ and finally another half timestep in $\mathcal{B}$. These operators $\mathcal{A}$ and $\mathcal{B}$ are defined below in §3.2 and §3.5.

3.2. Finite Volume Method

A finite volume method is used to solve the homogeneous equation of fluid motion (22). By discretising the domain into grid cells, we arrive at a description of flow in and out of control volumes. By enforcing equation (22) on the boundaries of these control volumes we arrive at a finite volume method.

To discretise equation (22), a *method of lines* approach is employed. The time-averaged change in a cell i is defined as:

$$\mathcal{L}(Q_i) = \frac{\mathcal{F}_{i+\frac{1}{2}} - \mathcal{F}_{i-\frac{1}{2}}}{\Delta x} \tag{25}$$

where $\mathcal{F}_{i+\frac{1}{2}}$ and $\mathcal{F}_{i-\frac{1}{2}}$ are the fluxes across the left and right boundaries of cell i, and $\mathcal{L}$ is the resulting update. This is the *conservative update formula*, and it ensures that the solution as a whole remains conservative.

With this estimate for the update $\mathcal{L}$ in each cell, a first order upwind method is applied to all of the cells in order integrate forward in time:

$$\mathbf{Q}^{n+1} = \mathbf{Q}^n + \Delta t^n \ \mathcal{L}(\mathbf{Q}^n) \tag{26}$$

To calculate the inter-cell fluxes $\mathcal{F}$, we consider the Riemann problem as sketched in figure 5. In a first order accurate method, the flux at the boundary $i + \frac{1}{2}$ is calculated as a function of the states Q_i and Q_{i+1} on either side:

$$\mathcal{F}_{i+\frac{1}{2}} = \mathcal{F}\left(Q_i,\ Q_{i+1}\right) \tag{27}$$

and for higher order methods, the stencil can be widened to include more cells on either side. In this project, for reasons of generality, a numerical flux function was used rather than a Riemann solver based method. However, it would not be difficult to upgrade the flux calculation to a Riemann solver method for future work. As can be seen in the comparison of results in §A.2, the approximate method compares favourably with the Riemann solver based method used by Kapila [20]. The methods used in this project are defined below.

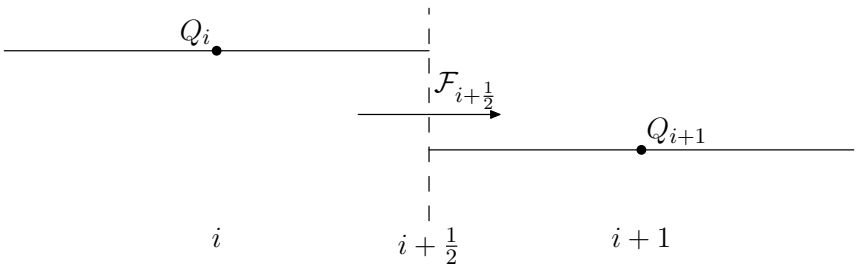

Figure 5: The Riemann problem on the boundary between cells i and $i+1$. The inter-cell flux $\mathcal{F}_{i+\frac{1}{2}}$ is calculated from the cell average values Q_i and Q_{i+1} on either side.

FORCE

The First ORder CEntred (FORCE) flux [38] is defined as an average of the first order Lax-Friedrichs flux and second order Richtmeyer flux. This results in a scheme that is first order accurate, but has minimal diffusion. At the interface of cells i and $i+1$, the FORCE flux is defined as:

$$\mathcal{F}^{LF\ n}_{i+\frac{1}{2}} = \frac{1}{2}\left(F(Q_i^n) + F(Q_{i+1}^n) + \frac{\Delta x}{\Delta t^n}\left[\ Q_i^n\ -\ Q_{i+1}^n\ \right]\right) \tag{28}$$

$$Q^\star = \frac{1}{2}\left(\ Q_i^n\ +\ Q_{i+1}^n\ + \frac{\Delta t^n}{\Delta x}\left[F(Q_i^n) - F(Q_{i+1}^n)\right]\right) \tag{29}$$

$$\mathcal{F}^{RI\ n}_{i+\frac{1}{2}} = F(Q^\star) \tag{30}$$

$$\mathcal{F}^{\ n}_{i+\frac{1}{2}} = \frac{1}{2}\left(\mathcal{F}^{LF\ n}_{i+\frac{1}{2}} + \mathcal{F}^{RI\ n}_{i+\frac{1}{2}}\right) \tag{31}$$

The full derivation of the FORCE flux can be found in Chap. 7 of Toro [38]. Since it is only first order, FORCE is too diffusive for most applications. However, it is the starting point for the second order SLIC method described below.

SLIC

The Slope LImited Centred (SLIC) scheme is a second order extension of the FORCE flux. SLIC is one of a class of methods known as 'Monotonic Upstream-Centred Scheme for Conservation Laws' or MUSCL [38].

In the FORCE method, the cell average data is extrapolated in a piecewise *constant* manner to the cell boundaries. The MUSCL approach uses piecewise *linear* extrapolation from the cell centres to the boundaries, thus providing better input data for the flux calculation. The slope for all cells i is calculated for each component q of the conserved vector by:

$$\Delta_i = \frac{1}{2}\left(q_{i+1} - q_{i-1}\right) \tag{32}$$

and this slope is used to calculate boundary values on the left and right of the cell:

$$q_i^L = q_i - \frac{1}{2}\Delta_i \qquad\qquad q_i^R = q_i + \frac{1}{2}\Delta_i \tag{33}$$

A potential problem with this approach is that it can introduce erroneous oscillations near sharp features. As illustrated in figure 6, the reconstructed values can lie outside the physical range of the solution.

To remedy this, a slope limiter function is applied. This function acts to reduce the interpolated gradient Δ_i (as calculated in (32)) in areas near discontinuities, so the method reduces to a constant extrapolation of the cell states. However, in regions of smooth flow, the slope is not limited and so that in such regions second order accuracy can be achieved.

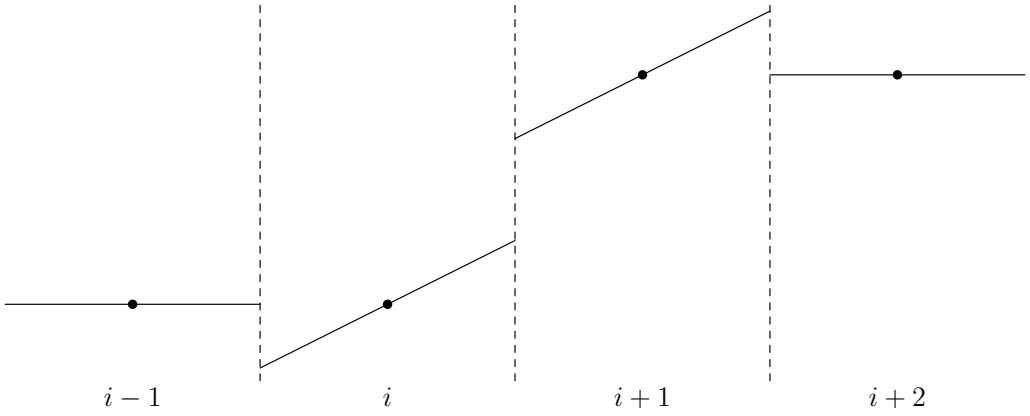

Figure 6: Piecewise linear reconstruction is used to extrapolate the cell centred values to the cell boundaries. This can lead to overshoots, as shown on the boundaries at $i - \frac{1}{2}$ and $i + \frac{3}{2}$.

Toro [38] lists four choices for the limiter function. In this report, the so called VANLEER function is used:

$$\xi(r) = \begin{cases} 0 & r \leq 0 \\ \frac{2r}{1+r} & r \geq 0 \end{cases} \tag{34}$$

and this is used to find the limited slope $\hat{\Delta}$ from the unlimited slope Δ:

$$\hat{\Delta}_i = \Delta_i \, \xi \left(\frac{q_{i-1} - q_i}{q_i - q_{i+1}} \right) \tag{35}$$

This limited slope is then used in equation (33) to find the extrapolated boundary values.

To further improve the accuracy of the method, these boundary values are then *centred* halfway through the timestep by:

$$\bar{Q}_i^L = Q_i^L + \frac{\Delta t}{2\Delta x} \left(F(Q_i^L) - F(Q_i^R) \right) \tag{36}$$

$$\bar{Q}_i^R = Q_i^R + \frac{\Delta t}{2\Delta x} \left(F(Q_i^L) - F(Q_i^R) \right) \tag{37}$$

Finally, to estimate the flux across the cell boundaries, these values $\bar{Q}^L$ and $\bar{Q}^R$ are used as inputs for a first order flux calculation. In the specific case of SLIC, the FORCE scheme described above is used:

$$\mathcal{F}_{i+\frac{1}{2}} = \mathcal{F}_{\text{FORCE}} \left(\bar{Q}_i^R, \; \bar{Q}_{i+1}^L \right) \tag{38}$$

3.3. Boundary Conditions

The final component of the numerical method is the treatment of the boundaries at each end of the simulated domain. *Ghost cells* are added at either end of the computation domain, with data from within the physical domain. This process is equivalent to a one-sided, first order formula.

The advantage of using ghost cells is that the spatial discretisation can be applied identically to the whole domain, and does not need adjusting near the boundaries.

The two types of boundary that we need to model are *transmissive* and *reflective*. To project into a transmitted ghost cell we simply copy the data over from inside the domain. To project into a reflected ghost cell, the momentum component is reflected and the other components are simply copied as before. For the piston impact experiments, the moving wall is simulated with a reflective boundary and the open end has a transmissive boundary.

3.4. Choice of Timestep

To determine the timestep Δt^n with which to advance the solution from t^n to t^{n+1}, the Courant-Friedrichs-Lewy (CFL) condition is applied. The CFL condition is a necessary condition that must be satisfied by any finite volume solver to ensure stability and convergence.

The CFL condition [10] states that:

> The numerical domain of dependence must contain the true domain of dependence of the partial differential equation, at least in the limit as Δt and Δx go to zero.

In practical terms for the type of explicit finite volume method applied here, this means that the speed at which information travels in the computational domain must be greater than the speed of the physical features that we wish to model.

Therefore, to satisfy this condition at timestep n, we require:

$$s^n_{max}\,\Delta t^n \leq \Delta x \tag{39}$$

where Δx is the spacing of the uniform computational grid and s^n_{max} is the wave speed of the fastest feature that we wish to evolve.

To use this condition to select Δt^n, the maximum wave speed on the domain must be calculated. If a solution to the Riemann problem is available, this wave speed can be found exactly. However, in this project, an approximate formula is applied. In a cell i, s_i is estimated:

$$s^n_i = |u^n_i| + a^n_i \tag{40}$$

s^n_{max} is then found by reducing over all the cells to find the maximum value of s^n_i. Finally, Δt^n can then be chosen according to the equation:

$$\Delta t^n = 0.9 \times \frac{\Delta x}{s^n_{max}} \tag{41}$$

The value 0.9 is chosen to ensure that condition (39) is met with some margin for safety.

3.5. Source Terms

To integrate the ordinary differential equation system in equation (23), the LSODE [28] package is used. LSODE is a collection of FORTRAN subroutines for numerical solution of initial value problems of the form:

$$\frac{\mathrm{d}\mathbf{y}}{\mathrm{d}t} = \mathbf{f}\Big(\mathbf{y}, t\Big) \tag{42}$$

where an initial condition $\mathbf{y}_0 = \mathbf{y}(t_0)$ is specified. $\mathbf{y}$ is a vector and t is an independent (time-like) variable.

The LSODE package contains several integration routines, and switches between them automatically according to the nature of the problem. For non-stiff systems, an implicit Adams method is applied and for stiff systems, backwards differentiation formulae are used. With a specified error tolerance, the package also chooses optimum values for its timestep and for the order of the integration.

4. Single and Compound Equations of State

In this section, we shall consider two different approaches to forming an equation of state to describe a mixture of fluids. The first option is to prescribe a *single* equation (in the form of JWL or similar), and use parameters that are fitted to the properties of the mixture. If the mixture is reactive, the equation of state can be augmented with a heat release term proportional to the volume fraction (λ) which describes the energy released in the reaction. The second option is to define separate equations of state for each fluid component and combine them using mixture rules to form a *compound* equation for the mixture.

There are several possible advantages and disadvantages to each approach. Using a single equation fitted to the mixture gives a simple equation that can be evaluated directly, whereas evaluating the compound equation can be difficult, requiring a numerical root finding procedure to satisfy the mixture rules. These mixture rules also introduce new physical assumptions, which have to be checked to ensure that they are valid.

The advantage of the compound equation is that by combining separate equations that have been fitted accurately to the pure fluid components, we might hope to be able to predict emerging features of the mixture. Another important aspect is that by combining equations for pure fluids with mixture rules, this methodology can in theory be extended to arbitrarily many mixing fluids.

To investigate and quantify these differences, the explosive nitromethane is investigated. The two different methodologies are presented in §4.1 and §4.2, and the results of some simulations of shock induced detonation are presented in §4.3.

4.1. Single Equation of State

To model the mixture of nitromethane and its reaction products, we can simply use the equation of state for nitromethane. This assumes that the products of the reaction behave identically to the unreacted nitromethane. To include a model for the heat released in the reaction, we augment the equation of state with a heat release term proportional to the reaction progress variable λ. λ varies from $\lambda = 0$, which signifies a pure state of reactants, to $\lambda = 1$, which signifies a pure state of products. Values outside the range of $[0, 1]$ are not meaningful.

The caloric equation of state for the nitromethane reactants has the form $e = e^\star(v, p)$. We shall use a JWL type equation with parameters defined by Tarver and Urtiew [37] - see table 1. The single equation of state is extended:

$$e = e^\star(v, p) + \lambda \mathfrak{Q} \tag{43}$$

where $\mathfrak{Q}$ is a constant defining the energy released in the reaction. Here,

$$\mathfrak{Q} = 1.44 \times 10^9 \,\mathrm{Pa} - \mathrm{cc/cc}$$

was chosen to obtain the measured steady state detonation velocity of nitromethane, which is 6234 m/s [14]. It is not necessary to define a thermal equation of state for the mixture, as the temperature of the mixture is not required.

The Hugoniot for the reactants and the Crussard curves for the simulated detonation products representing the various (p, v) states for this material are plotted in figure 7. The Hugoniots are plotted for $\lambda = 0 \rightarrow 1$ in steps of 0.2. Also shown is the Rayleigh line, which is tangential to the Crussard curve with λ equal to 1 at the state $(p, v) = (0.243, 0.758)$.

4.2. Compound Equations of State

The methodology for defining a mixture equation of state from two (or more) equations for component materials is discussed more thoroughly in §5. Above, in §4.1, the variable λ is a reaction progress variable, but in this formulation, it will be defined as the volume fraction of the reactants and products. It is again defined on the interval $[0, 1]$, with $\lambda = 0$ specifying a pure state of reactants and $\lambda = 1$ specifying a pure state of products.

The same JWL equation from §4.1 will be used for the reactants, and a second JWL equation is used for the products. As above, we use the parameter sets defined by Tarver [37] - (see table 1).

To close the mixture rules that define the mixture equation of state, the two fluids are assumed to be in temperature equilibrium. The physical implications of this assumption will be further discussed in §5.

The Hugoniot for the reactants and the Crussard curves for the detonation products representing the various (p, v) states for this material are plotted in figure 8. The Hugoniots are plotted for $\lambda = 0 \rightarrow 1$ in steps of 0.2. Also shown is the Rayleigh line, which is tangential to the Crussard curve with λ equal to 1 at the state $(p, v) = (0.287, 0.714)$.

In figure 8, the Hugoniots are seen to intersect for pressures greater than ~ 0.55 (in the scaled units). This indicates that the equations of state are no longer valid at these pressures. However, this compression is above the von Neumann spike and so the simulation will not enter this region.

Comparing figures 7 and 8, it can be seen that the Hugoniot for the reactants (in blue) is identical. The Crussard curve for the products is much flatter in figure 8, which is a better representation of the relatively easily compressed gas phase. The Hugoniots for the mixed phases are also flatter. This means that the compound equation of state gives a more physical model for the mixture of liquid reactants and gaseous products.

Figure 8 also shows the evolution of the mixture volume and the partial volumes of the solid and gas phases along the Rayleigh line.

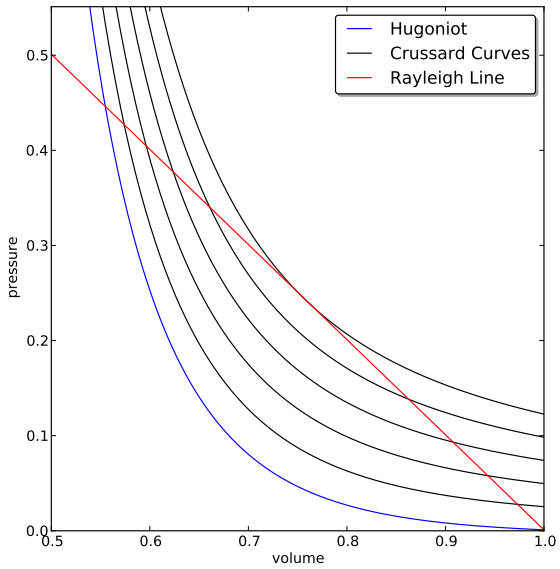

Figure 7: Mixture analysis for nitromethane with one JWL equation of state augmented with heat release term.

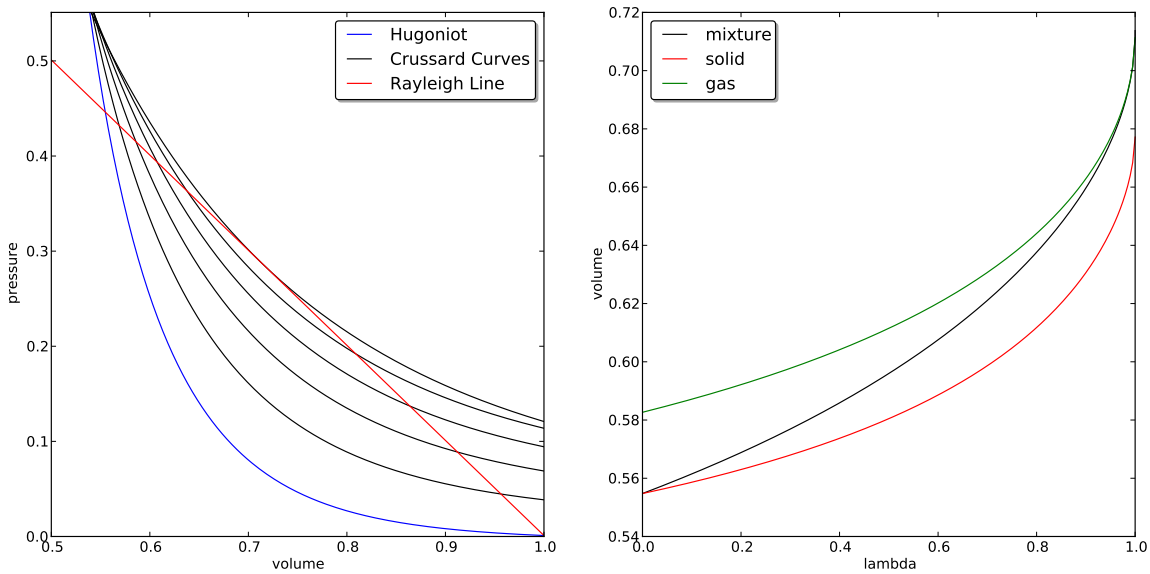

Figure 8: Mixture analysis for nitromethane with two JWL equations of state. Temperature equilibrium is used to close the mixture.

4.3. Piston Impact Results for Nitromethane

To further investigate the difference between the use of the single and compound equations of state, piston impact simulations were performed to reproduce the results of an experiment by Dattelbaum et al.[11]. Dattelbaum's results are shown in figure 9.

These results are obtained from a series of electromagnetic gauges that are embedded in the material. These gauges give particle velocity measurements at nine Lagrangian positions. The first gauge (in black) shows the input shock, the next four gauges describe the ignition phase of the evolution and the final four gauges show a steady state travelling detonation wave.

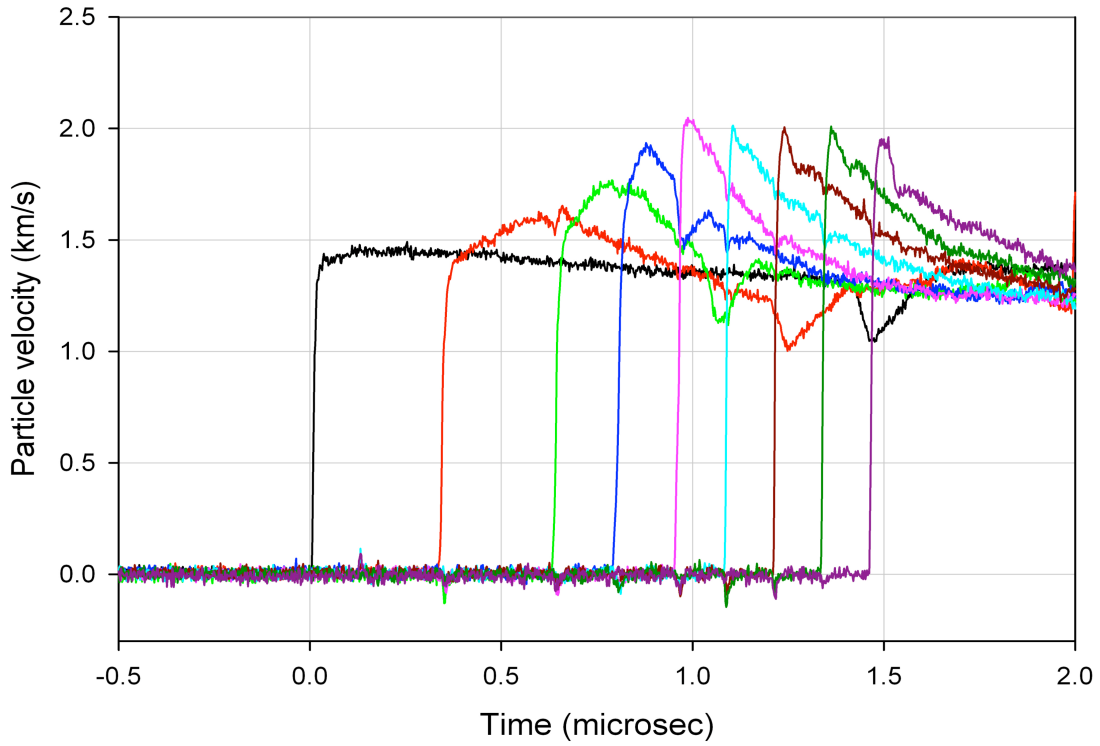

Figure 9: Particle velocity measurements for a piston impact experiment on nitromethane performed by Dattelbaum et al. [11, fig. 7].

Two simulations were performed with the single and compound equations of state and the results are shown in figures 10 and 11 respectively. The results are presented to mimic the measurements provided by the Lagrangian measurement technique, with nine marker particles set at starting positions: 0.0, 0.1, 0.2, 0.266, 0.333, 0.4, 0.466, 0.533 and 0.6 (scaled units). Unfortunately, Dattelbaum et al. do not specify the starting position of the gauges in their experiment, but these positions were found to give similar results. Dattelbaum et al. specify an input pressure of 8.2 GPa and this was used to specify the impact velocity 0.2625 (scaled units) for the simulation. The two simulations were both run with 1600 grid cells covering the domain. This value was chosen following a convergence study.

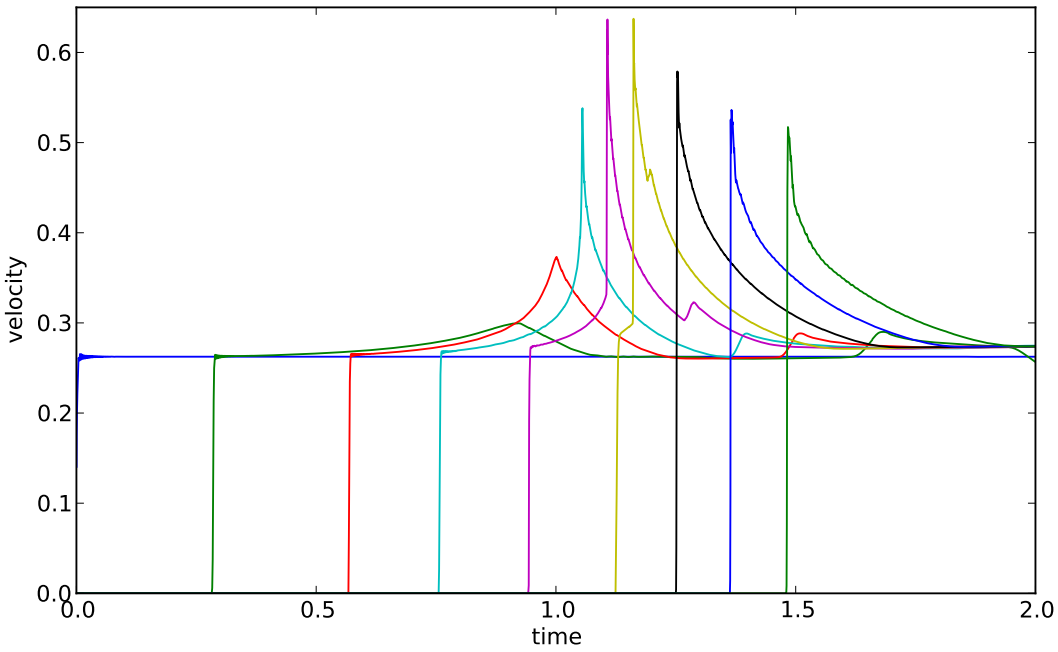

Figure 10: Particle velocity measurements for a piston impact simulation on nitromethane with one equation of state. The simulation was run in 1600 grid cells and the values are given in the scaled units.

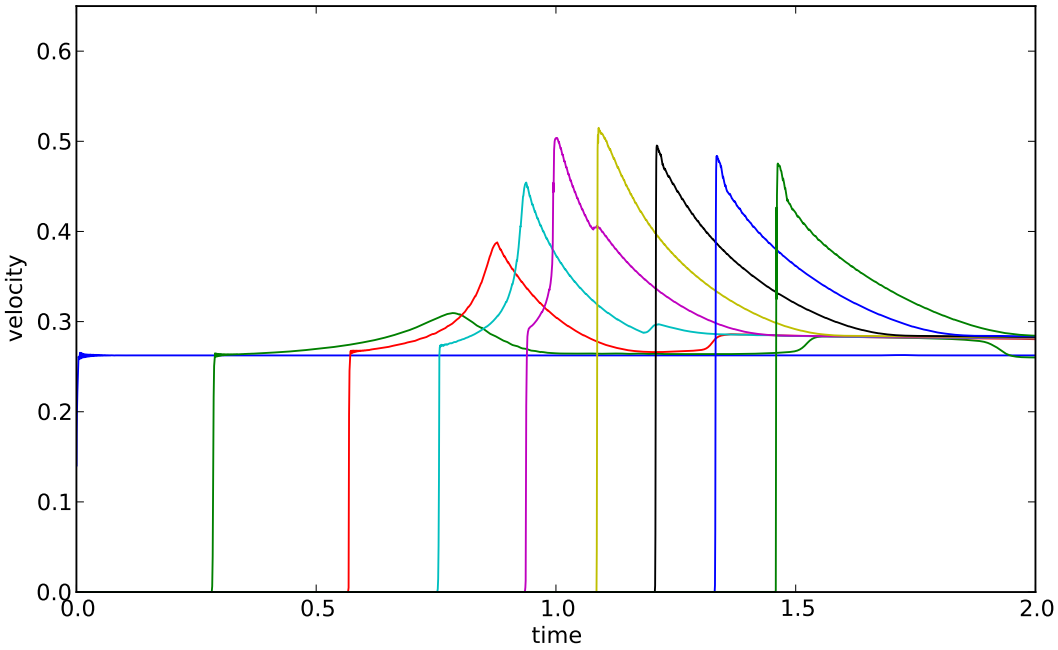

Figure 11: Particle velocity measurements for a piston impact simulation on nitromethane with two equations of state. The simulation was run in 1600 grid cells and the values are given in the scaled units.

In both the single and compound equation of state simulations, the detonation occurs at around $1\,\mu$s. This matches the result of the experiment. The main difference between the two set of results is the height of the overdriven detonation peaks: in the single equation of state results, the velocity goes over 0.6 in the scaled units ($\sim 3.8\,$km/s) and in the compound equation of state results, the same peak just reaches 0.5 in the scaled units ($\sim 3\,$km/s). The reference velocity used to scale the values in this simulation is 6243.2 m/s and the reference time is $1\,\mu s$. While both values are too high, the compound results are much closer to the results of the experiment.

In the experimental results, the particle velocities are steadily decreasing. This effect is not seen in the simulations, as the one dimensional approximation does not model the energy loss in the radial direction. While the simulations do not exactly match the experimental results, the compound equation of state results in particular qualitatively capture all of the important features of the evolution.

4.4. Discussion

The results of the simulations presented above show that both the single and compound equation of state for nitromethane give reasonable results. The compound approach gives the more accurate results at the expense of computational complexity. The single equation approach might be expected to work well in situations where the two fluid components have similar properties. In this case, one component is liquid and the other is gaseous, so the single equation approach does not perform so well.

In simulations involving three or more materials, a combination of both methodologies can be applied. In the simulations of LX-17 in §5, four materials are present. In this case, we use one equation of state for the reactants, which is a mixture of explosive TATB crystals and solid plastic binder and a second equation of state for the mixture of product gases and vaporised binder. The solid and gas equations of state are combined using mixture rules.

5. Compound Equations of State

In this study, we consider models of the form introduced in §2.2. Two phases of the fluid are evolved and we make the assumption that the phases are in pressure equilibrium ($p = p_s = p_g$) and are moving with the same velocity.

Petitpas [27] has calculated the timescale for pressure equilibrium, and finds that it is of the order of 10^{-8} seconds. This is similar to the timestep required by the CFL condition dictated by the timescales in the dynamics of the problem. Thus, it is a reasonable assumption that pressure equilibrium applies everywhere at each timestep.

We define the specific volume of the mixture (v) as a weighted sum of the two phase volumes v_s and v_g and the specific internal energy (e) as a similar weighted sum of the two specific internal energies, e_s and e_g:

$$v = v_s\,(1-\lambda) + v_g\lambda \qquad e = e_s\,(1-\lambda) + e_g\lambda \tag{44}$$

These equations are usually referred to as the *mixture rules*. Here, λ is the volume fraction of the gaseous product phase and $(1-\lambda)$ is the volume fraction of the solid reactants. λ is given by the solution of the augmented Euler equations (5). Following Stewart et al. [34], it is convenient to write the ratios of these volumes as:

$$\phi = \frac{v_s}{v_g} \tag{45}$$

which gives the partial volumes:

$$v_s(\phi) = \frac{\phi v}{\lambda + (1-\lambda)\phi} \tag{46}$$

$$v_g(\phi) = \frac{v}{\lambda + (1-\lambda)\phi}\,. \tag{47}$$

This parameterisation allows the root finding procedures described below to be applied to the auxiliary parameter ϕ rather than to the partial volumes directly. This is advantageous, as ϕ is much better behaved than the two partial volumes.

The separate phases are assigned separate equations of state. To define the mixture equation of state by combining the two individual equations of state, a further assumption needs to be made about the energy exchange between the solid and gas phases. We consider three possibilities for this assumption to close the system:

1	Temperature equilibrium
2	Constant volume ratio
3	Thermal isolation

In the following subsections, these three closure conditions are presented. The three assumptions are applied to form mixture equations of state for LX-17, and in §5.4 and §5.6 the effect of applying the different conditions to the same piston impact problem is investigated.

5.1. Temperature Equilibrium

The most common method of closure is temperature equilibrium. Petitpas [27] has calculated the relaxation timescales for typical explosive materials to reach temperature equilibrium to be of the order of 10^{-4} seconds. However the dynamics of the problem are much faster than this and the CFL condition requires a timestep of less than 10^{-8} seconds. So the time to reach temperature equilibrium is at least of the order of thousands of timesteps. Indeed, a typical detonation wave traveling at 10^3 m/s will have travelled the length of the experiment before this condition is satisfied - so the temperature equilibrium cannot be reached before the phenomenon we are trying to model has passed.

In spite of this inconsistency, temperature equilibrium is the standard approach for closure and so it is included here as a benchmark for comparison.

This physical condition is enforced by requiring that:

$$T_s(v_s, p) = T_g(v_g, p) \tag{48}$$

where T_s and T_g are the thermal equations of state for the solid and gaseous phases respectively.

This relation specifies a value of ϕ at each time step which can be found as the root of:

$$f(\phi) = T_s\left(v_s(\phi), p\right) - T_g\left(v_g(\phi), p\right) = 0 \tag{49}$$

where the equations (46) and (47) are used to relate the auxiliary parameter ϕ to the partial volumes of the solid and gas phases. This root is found by iteration using the Newton-Raphson method. This numerical approach was used, as an analytical solution is only possible for simple equations of state such as ideal gas.

The Hugoniot for the reactants and the Crussard curves for the detonation products representing the various (p, v) states for this closure condition are plotted in figure 12. The Hugoniots are plotted for $\lambda = 0 \rightarrow 1$ in steps of 0.2. Also shown is the Rayleigh line, which is tangential to the Crussard curve with λ equal to 1 at a specific volume of 0.75. This indicates that the detonation has achieved the Chapman-Jouguet state.

It can also be seen that the Crussard curves intersect at a specific volume of just less than 0.7, indicating that the equation of state not valid below this value. However, the largest possible compression is at the von Neumann state at $v = 0.69$, so the simulation is in any case not physically meaningful below this value.

The evolution of the mixture volume and the specific volumes for the solid and gas phases along the Rayleigh line is also shown in figure 12. It can be seen that the two phases are both compressed similarly. This is physically incorrect as the gas should be compressed more than the solid.

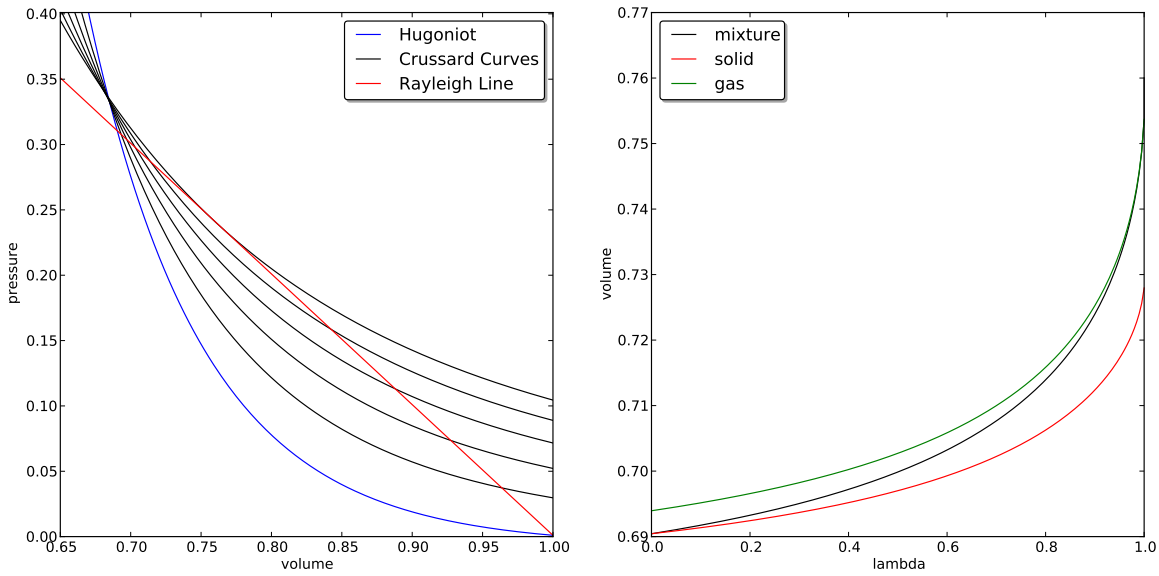

Figure 12: Mixture analysis for LX-17 calculated with temperature equilibrium. The volume is scaled to the initial state.

5.2. Constant Volume Ratio

A computationally simple way of performing the closure is to impose a constant value for ϕ. This idea was suggested by Stewart [34].

The constant ϕ is chosen from the range of values calculated by the temperature equilibrium procedure above. Values in the range $0.85 \rightarrow 1.0$ were tested to find a suitable detonation structure. In practice the value needs to be tuned for each simulation. In the simulations presented below in §5.4, the value used is $\phi = 0.98$ as this gave a good detonation structure.

The Hugoniots for this closure condition are plotted in figure 13. As above, the Hugoniots are plotted for $\lambda = 0 \rightarrow 1$ in steps of 0.2. Again, the Rayleigh line is tangential to the Crussard curve with λ equal to 1 at a specific volume of just over 0.75. The curves for the pure states at $\lambda = 0$ and 1 are of course identical to the corresponding curves in figure 12. The curves for the intermediate values of λ appear to be very similar but are in fact subtly different. The difference is more apparent in the plot of the volumes. The partial volume of the solid behaves physically better (i.e. does not compress) for $\lambda < 0.5$ but for $\lambda > 0.5$ the solid compresses unphysically as above. However the reverse is true for the partial volume of the gas: for $\lambda > 0.5$, the gas compresses as required, but behaves unphysically (i.e. does not compress) for $\lambda < 0.5$.

5.3. Thermal Isolation

The third method of closing this system of equations is to assume that the two phases are in thermal isolation. To enforce this physical assumption, we start from the basic axioms of thermodynamics:

$$đe = đ\mathcal{Q} - p\ đv \tag{50}$$

where e is the internal energy of the system, $đ\mathcal{Q}$ is the heat exchanged with the system and $p\ đv$ is the work done on the system. If the system is taken to be the solid phase of the mixture, the thermal isolation of the phases can be specified by setting $đ\mathcal{Q} = 0$. This leads to the differential equation defining the *isentrope*:

$$\frac{\partial e}{\partial v} = -p \tag{51}$$

into which the equation of state for the solid phase $p = p(v_s, e_s)$ can be inserted. Solving this defines a function $e_s = e_i(v_s)$ for the energy on the isentrope, which can be re-inserted into the equation of state to find a function for the pressure on the isentrope:

$$p = p_i(v_s) \tag{52}$$

This function is then used to close the system by setting the pressure of the mixture equal to the pressure of the solid on its isentrope. This is termed *isentropic closure*.

To implement this, we again use the Newton-Raphson iterative method to find the root of the function $f(\phi)$:

$$f(\phi) = p - p_i\left(v_s(\phi)\right) = 0 \tag{53}$$

where the relation in equation (46) is used, and equation (47) gives the partial volume of the gas phase.

The process of solving equation (51) and finding the root of equation (53) can be extremely time consuming for a complex equation of state. However, if the equation is in Mie Grüneisen form, the pressure and energy on the isentrope is defined by the reference curves, thus simplifying the process.

The Hugoniots for this closure condition are plotted in figure 14. Many of the same features are observed in the plot of the Hugoniots, and again the mixed Crussard curves appear very similar to the other two cases in figures 12 and 13.

In the plot of the partial volumes, it can be seen that the mixture behaves more physically under compression, for both phases and for all values of λ. In particular, the solid phase is much less compressed than the gas. Therefore, this assumption is the most physically realistic of the three. Despite this advantage, it is rarely used due to the complexity of implementing the scheme in a non steady-state hydrocode.

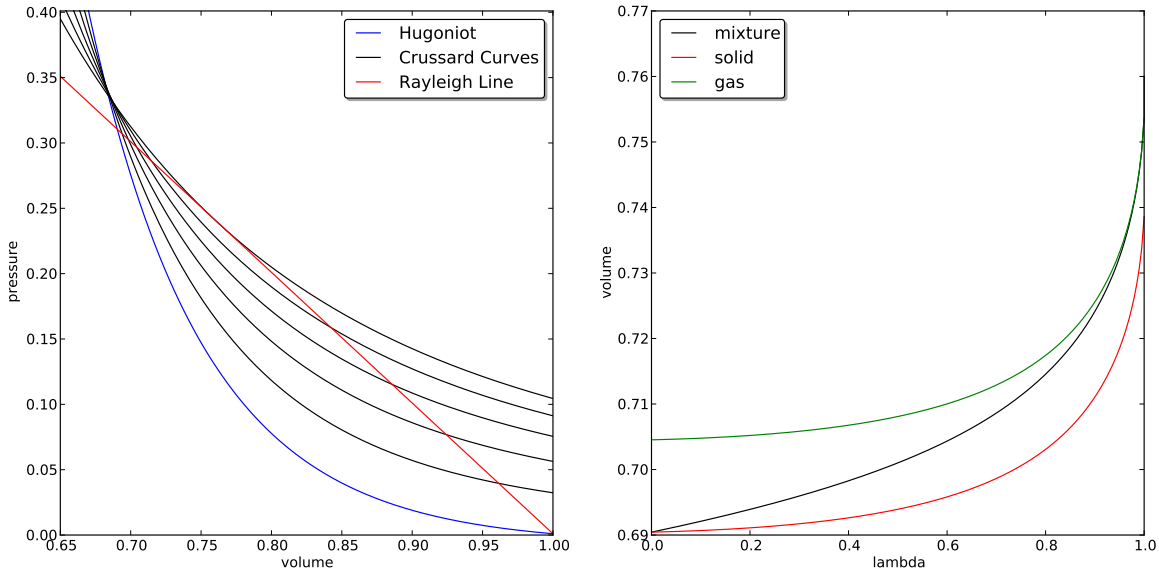

Figure 13: Mixture analysis for LX-17 calculated with constant volume ratio.

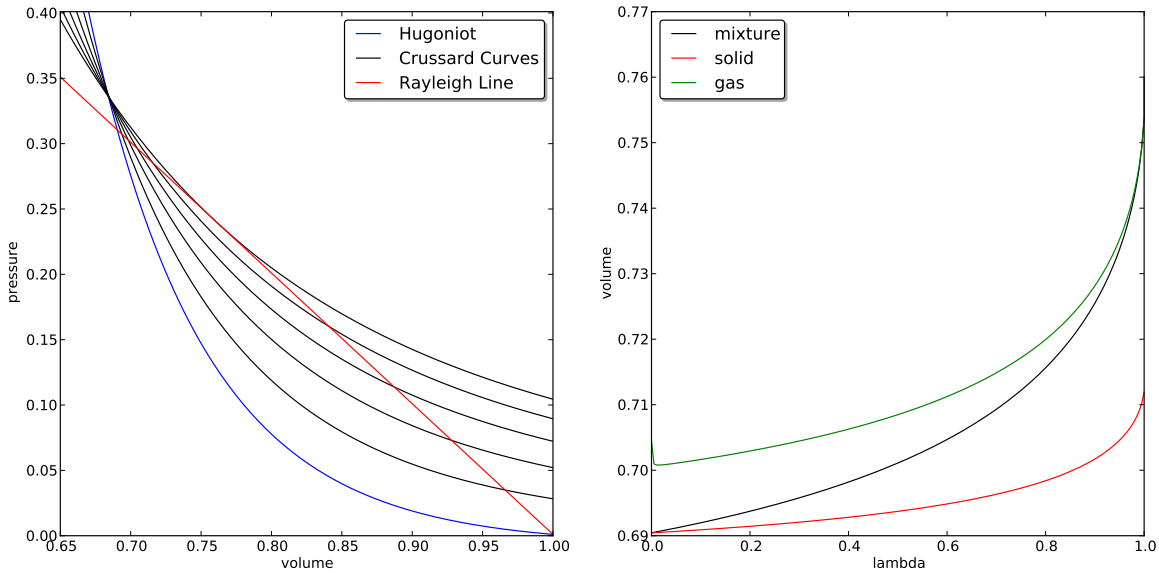

Figure 14: Mixture analysis for LX-17 calculated using isentropic closure.

5.4. Piston Impact Results for LX-17

To investigate the effect of the three different closure assumptions, piston impact simulations were performed. Following Kapila et al. [20], the widely studied heterogeneous explosive LX-17 is simulated with two JWL equations of state (see §2.3), and the ignition and growth reaction rate (§2.4). Kapila choses two test cases: a low speed, weak piston impact and a higher speed, strong piston impact designed to mimic an experiment by Gustavsen et al. [17]. The impact velocities in scaled units are given in table 5.

Experiment	Impact Velocity
Low speed	0.14
High speed	0.1888

Table 5: Parameters for Kapila's two test cases.

The experiments cause different wave structures. The first (low speed) case is a heterogeneous detonation where the shock caused by the impact initiates the reaction. The reaction initially spreads slowly, and gradually builds into a detonation wave. The detonation wave then catches up with the initial shock and overtakes it.

The second case has a higher impact speed which causes a homogeneous ignition. The impact shock initiates the reaction directly behind the shock, and the detonation wave grows directly out of the shock which speeds up as it approaches the steady state solution.

These two cases are illustrated in figure 15. In both diagrams, the dashed line indicates the precursor shock, which hits at $t = 0$. In the heterogeneous case (figure 15a), this shock continues, and during the red stage, the reaction is spread slowly by combustion. Then, in the blue stage, the reaction forms the detonation wave, which during the yellow time overtakes the precursor shock. It quickly settles down to the steady state in the green stage. In figure 15b showing the homogeneous case, the reaction builds out of the precursor shock in the red stage before forming the steady state detonation in the green stage.

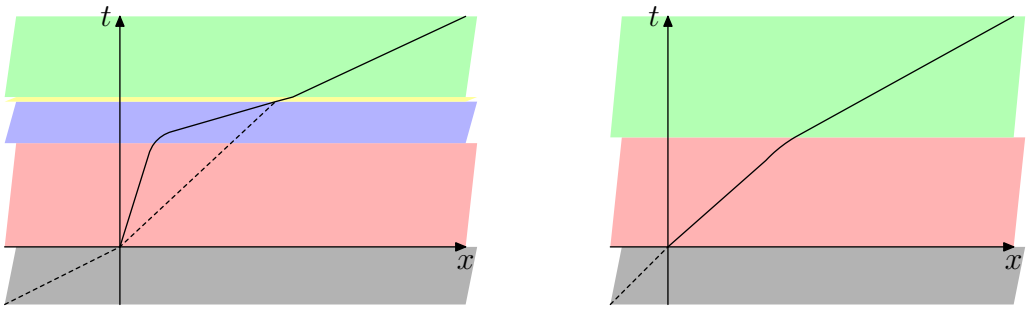

(a) Heterogeneous case.

(b) Homogeneous case.

Figure 15: Comparison of heterogeneous and homogeneous shock induced detonation [7, 8].

In order to determine the necessary resolution for the simulations, an initial grid convergence study was carried out at a time in the steady state phase of the evolution. The results for grid resolutions of 600 to 2400 cells are shown in figure 16, where it can be seen that the features of the Zel'dovich-von Neumann-Döring (ZND) pressure peak are clearly resolved for numbers of cells greater than 1800. Therefore, the simulations below have been run with each region divided into 2000 grid cells.

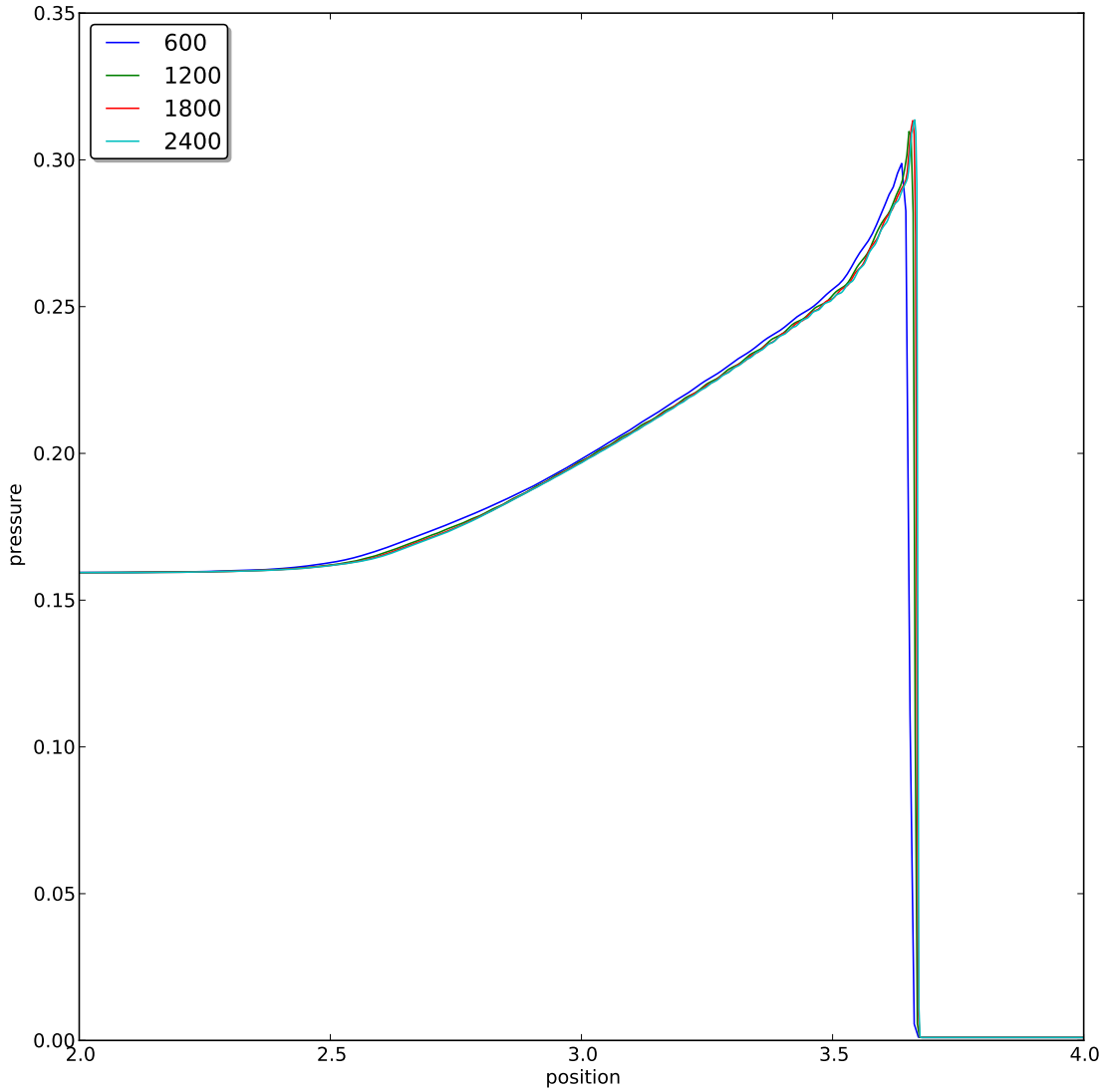

Figure 16: Results showing the convergence for 600, 1200, 1800 and 2400 cells for a steady state detonation wave.

Low Speed Impact

The results for the piston impact simulation are presented in two stages: initial ignition and steady state conditions. The initial *ignition* stage is shown for the three different closure conditions in figures 17, 19 and 21. In these figures the time evolution is indicated by superposing curves of different colours for times from 0.1 to 1.3 in steps of 0.1 (13 curves), and then from 1.3 to 1.7 in steps of 0.05 (8 curves). The precursor shock speed can be seen to be constant (about 0.52) throughout this period.

The longer evolution to steady state is shown in figures 18, 20 and 22. In these figures, the time evolution is indicated by superposing curves of different colours for times from 2.5 to 6.5 in steps of 0.5 (9 curves). The speed of the detonation wave can be seen to be constant (about 0.86) throughout this period. The final curve shows that the tube contains only gas.

The simulations performed using the temperature equilibrium assumption (figures 17 and 18) can be verified against the results from Kapila [20]. This comparison is shown in §A.2: excellent agreement was obtained.

All three closure methods produce broadly similar, physically meaningful, results - for further discussion see §5.5.

It can be seen that the lower speed piston impact causes a heterogeneous ignition and run to detonation. In the plots of the ignition stage, the precursor shock moves through the bulk of the material with no immediate effect. However, behind the shock, the reaction has started and energy is being liberated into the material. This energy causes a buildup in pressure, which starts at the interface with the piston and travels in towards the interior of the material. This wave steepens and grows in amplitude, forming a detonation wave which follows the lead shock.

In the later stages of the experiment, this detonation wave overtakes the precursor shock. After some transient effects, the wave settles to a steady state. This is the Chapman-Jouguet state, as verified by comparing values from the simulations with the mixture analysis curves in figures 12, 13 and 14.

High Speed Impact

The second simulation is a higher speed piston impact. As before, the results for the three closure conditions are split into the two stages of ignition and steady state. The ignition stage results are shown in figures 23, 25 and 27. In these figures the time evolution is again shown by superposing curves of different colours for times from 0.02 to 0.34 in steps of 0.02 (19 curves). The precursor shock speed can be seen to increase from about 0.58 at the start to about 0.77 at the end of the time period.

The results at later times when the detonation has settled to a steady state are shown in figures 24, 26 and 28. In these figures the time evolution is shown by superposing curves of different colours for times from 0.4 to 1.5 in steps of 0.1 (12 curves). The shock speed

can be seen to be constant (about 0.81) for this time period. The final curve shows that the tube is full of gas.

As above, the results generated here for temperature equilibrium (figures 23 and 24) can be directly compared with those from Kapila [20]. This comparison is shown in §A.2, and again, excellent agreement is observed.

Again all three closure methods produce broadly similar physically meaningful results - for further discussion see §5.5.

This impact is at a sufficiently high energy to cause a homogeneous detonation. The pressure peak caused by the reaction again forms at the wall and travels into the interior of the material. However, instead of the detonation forming a secondary shock wave, the detonation wave is directly attached to the lead shock which grows towards the characteristic profile of the ignition and growth model.

5.5. Comparison of Closure Conditions

Towards the end of the evolution, when the detonation wave has formed the steady Chapman-Jouguet state, it is seen that all three closure conditions give very similar results. Particularly in the high speed case, the results are indistinguishable.

In the ignition stage, some differences are observed. For the low speed case, the different closure conditions cause a variation in the sensitivity of the material. The results show that the whilst the precursor shock moves identically, the subsequent detonation wave forms at different times. The isentropic closure condition forces energy to stay in the solid reactants, so the reaction rate is faster. The constant ϕ results are very similar. However, for the temperature equilibrium assumption, energy is transferred away from the reactants, slowing the reaction rate.

There are other noticeable differences in the results for the ignition stage of the low speed test case. In particular, we see that the isentropic closure results have a pre-detonation pulse. This unexpected feature comes from an interaction with the complex form of the ignition and growth reaction rate. The 'ignition' term of the reaction rate causes a detonation rather than the intended ignition, again because the energy is forced to stay in the reactants. This is a result of the choice of parameters in the reaction rate. If the parameters were fitted to the isentropically closed model, one would expect this feature to disappear.

For high speed case, the differences between the closure conditions are less noticeable in the ignition stage. As the energy in the system is much higher, the effects of changing the exchange of energy between the phases are not so visible.

In order to pin down the effects of changing the closure condition and remove the complex interaction with the ignition and growth reaction rate, we now consider similar simulations with a simplified reaction rate.

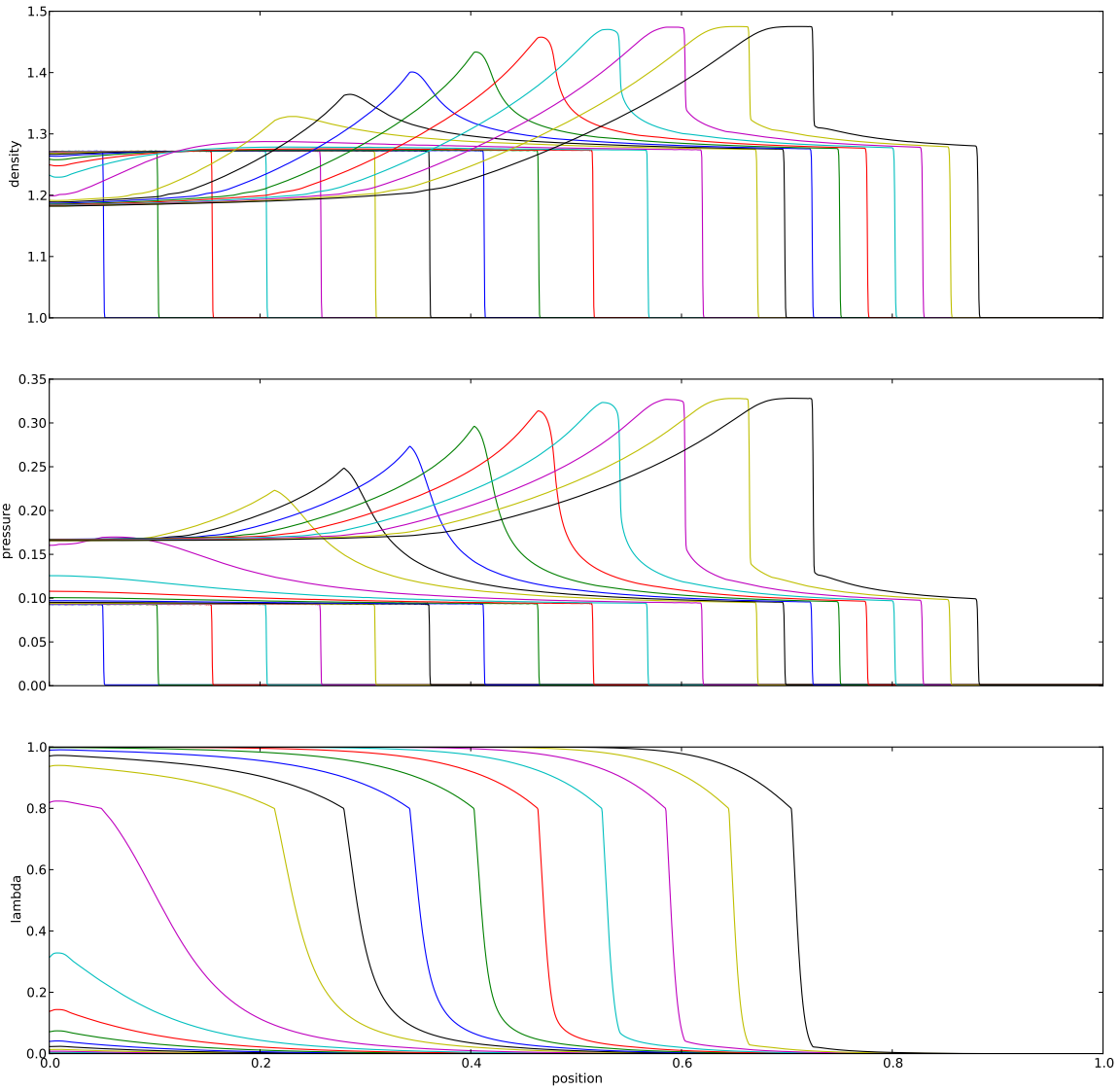

Figure 17: Low speed piston impact experiment on LX-17. Results plotted at times from 0.1 to 1.3 in steps of 0.1 and 1.3 to 1.7 in steps of 0.05 to show the ignition stage. The simulation was run in 2000 grid cells (between 0 and 1) with temperature equilibrium.

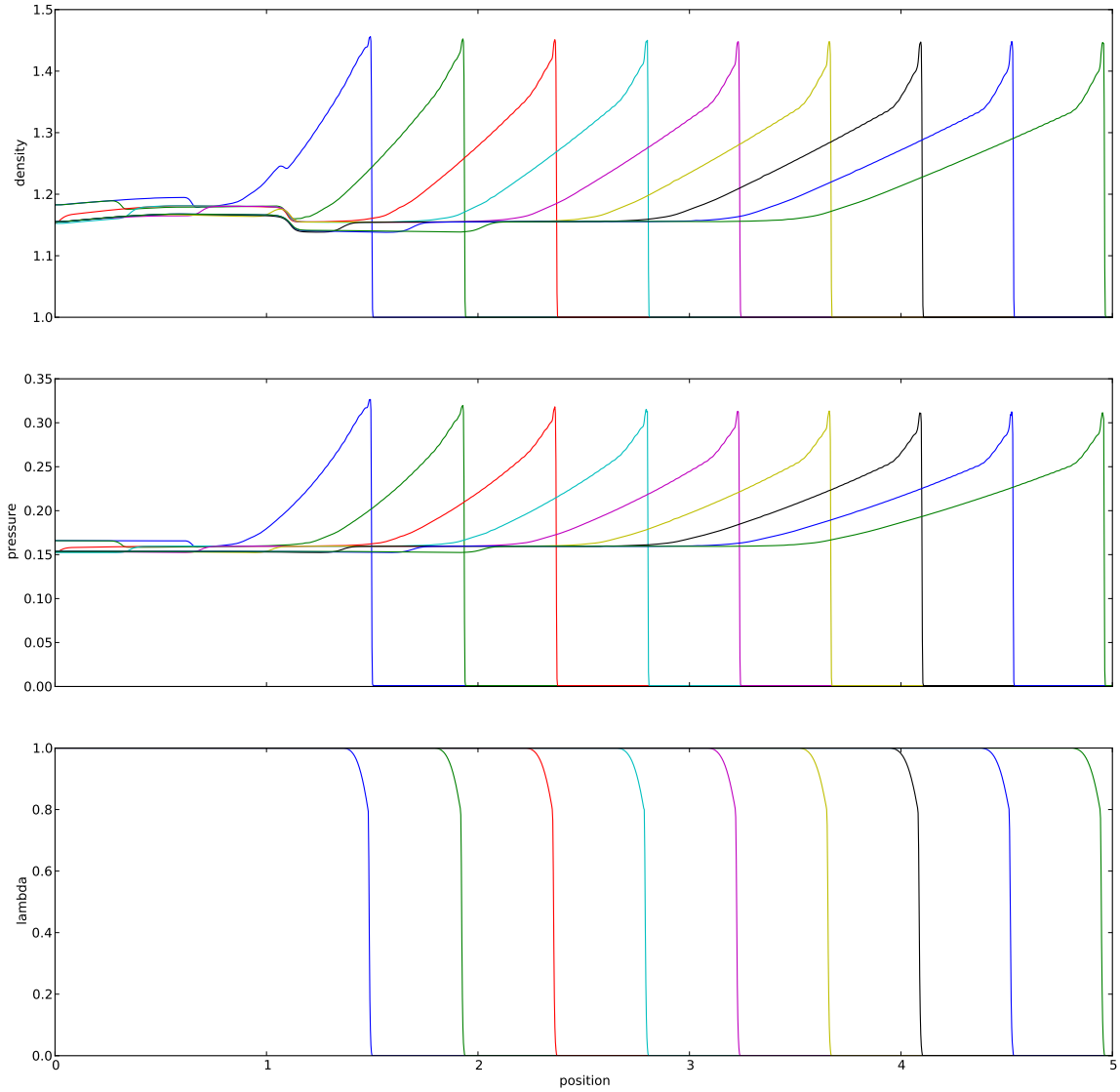

Figure 18: Low speed piston impact experiment on LX-17. Results plotted at times from 2.5 to 6.5 in steps of 0.5 to show the steady state stage. The simulation was run in 2000 grid cells (between 0 and 5) with temperature equilibrium.

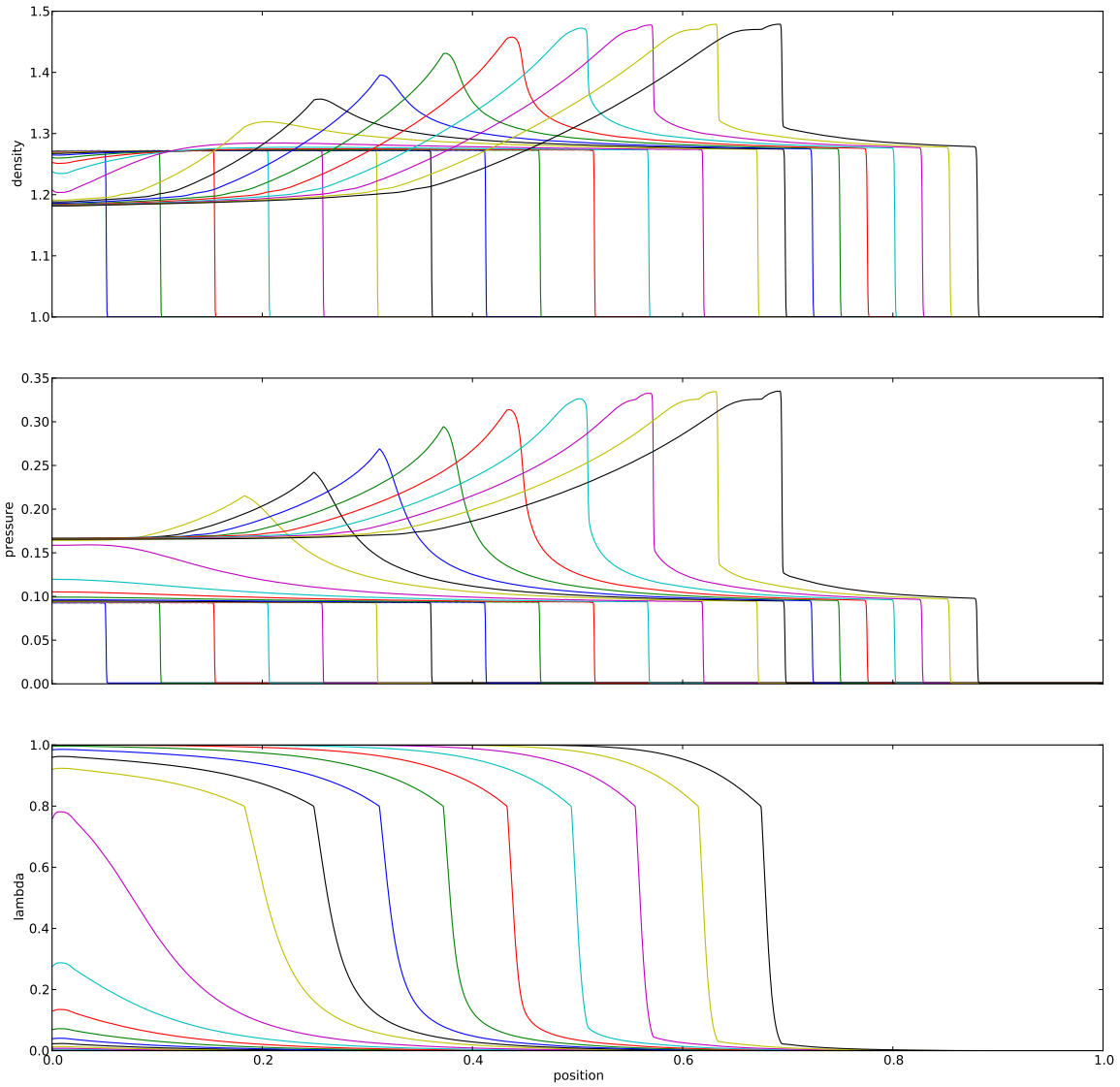

Figure 19: Low speed piston impact experiment on LX-17. Results plotted at times from 0.1 to 1.3 in steps of 0.1 and 1.3 to 1.7 in steps of 0.05 to show the ignition stage. The simulation was run in 2000 grid cells (between 0 and 1) with the constant volume ratio approximation.

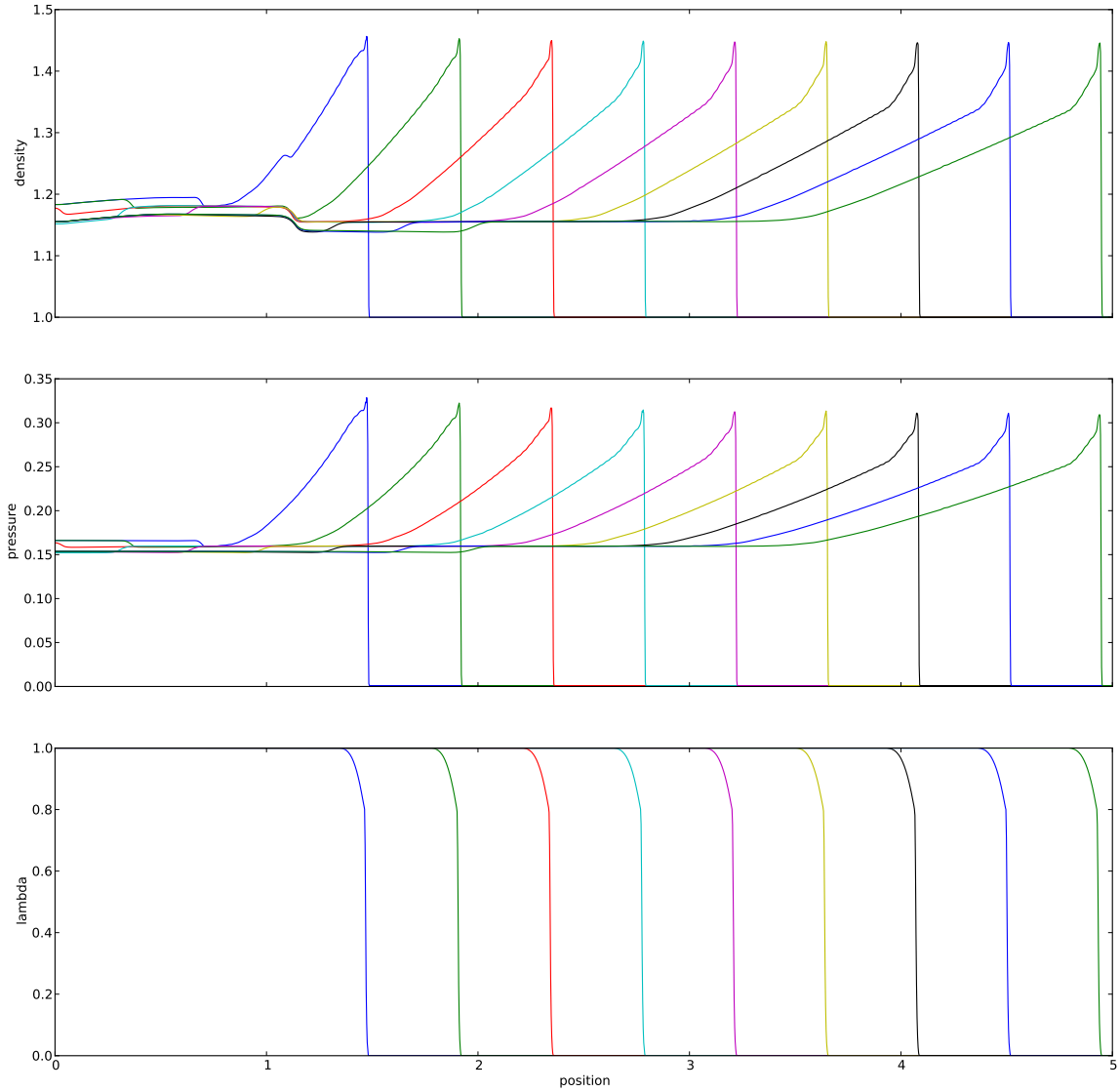

Figure 20: Low speed piston impact experiment on LX-17. Results plotted at times from 2.5 to 6.5 in steps of 0.5 to show the steady state stage. The simulation was run in 2000 grid cells (between 0 and 5) with constant volume ratio approximation.

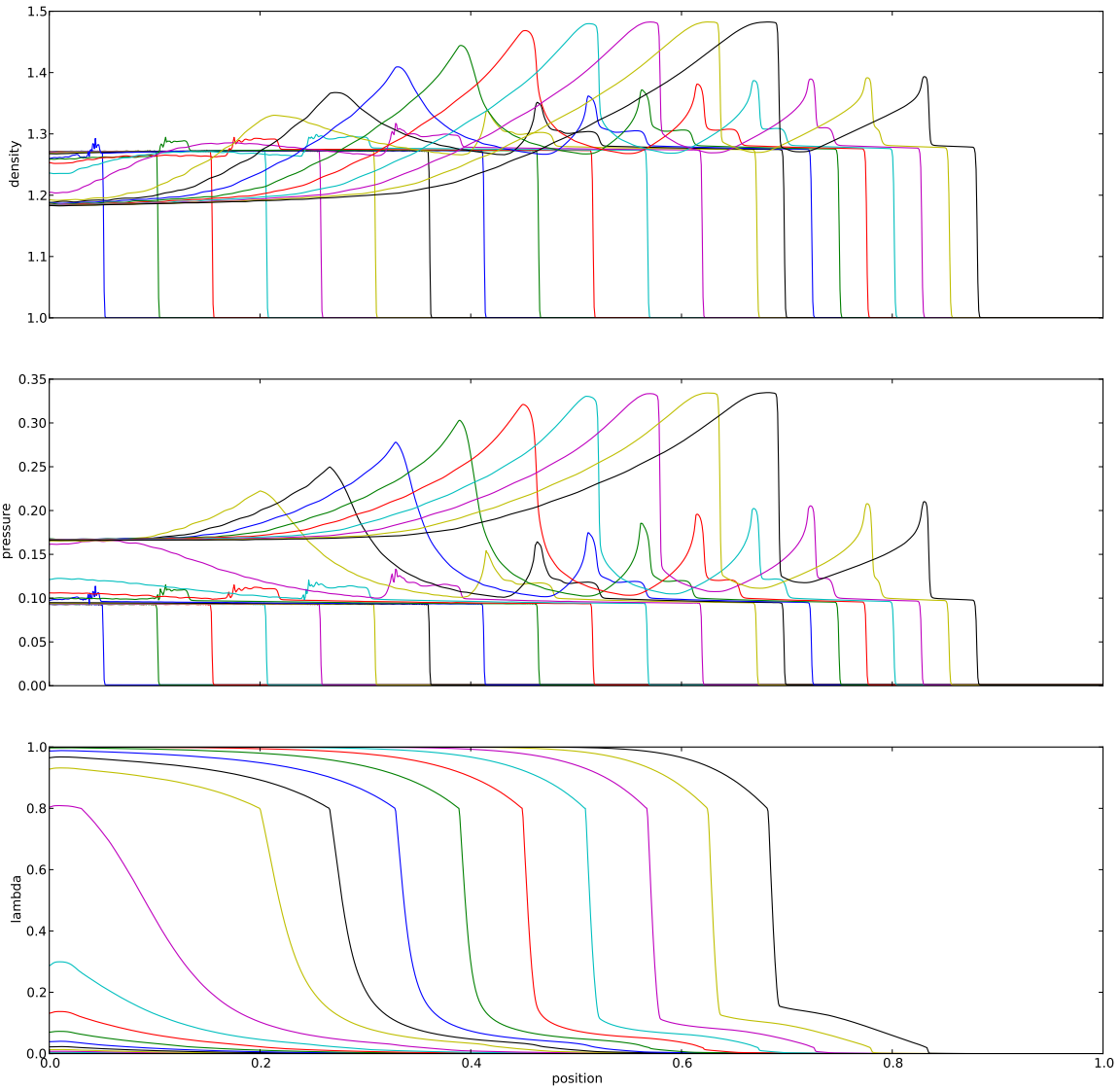

Figure 21: Low speed piston impact experiment on LX-17. Results plotted at times from 0.1 to 1.3 in steps of 0.1 and 1.3 to 1.7 in steps of 0.05 to show the ignition stage. The simulation was run in 2000 grid cells (between 0 and 1) with isentropic closure (thermal isolation).

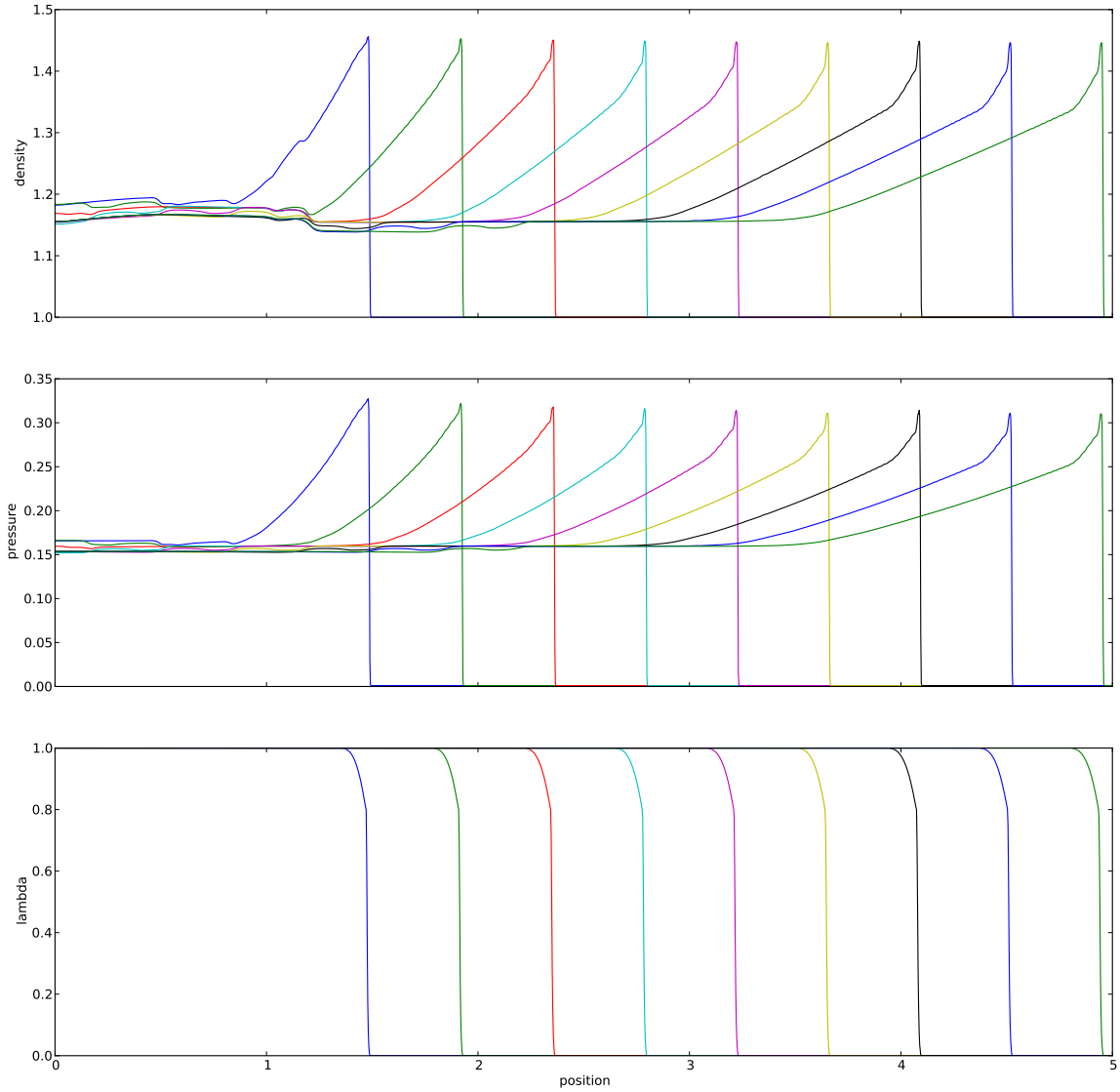

Figure 22: Low speed piston impact experiment on LX-17. Results plotted at times from 2.5 to 6.5 in steps of 0.5 to show the steady state stage. The simulation was run in 2000 grid cells (between 0 and 5) with isentropic closure (thermal isolation).

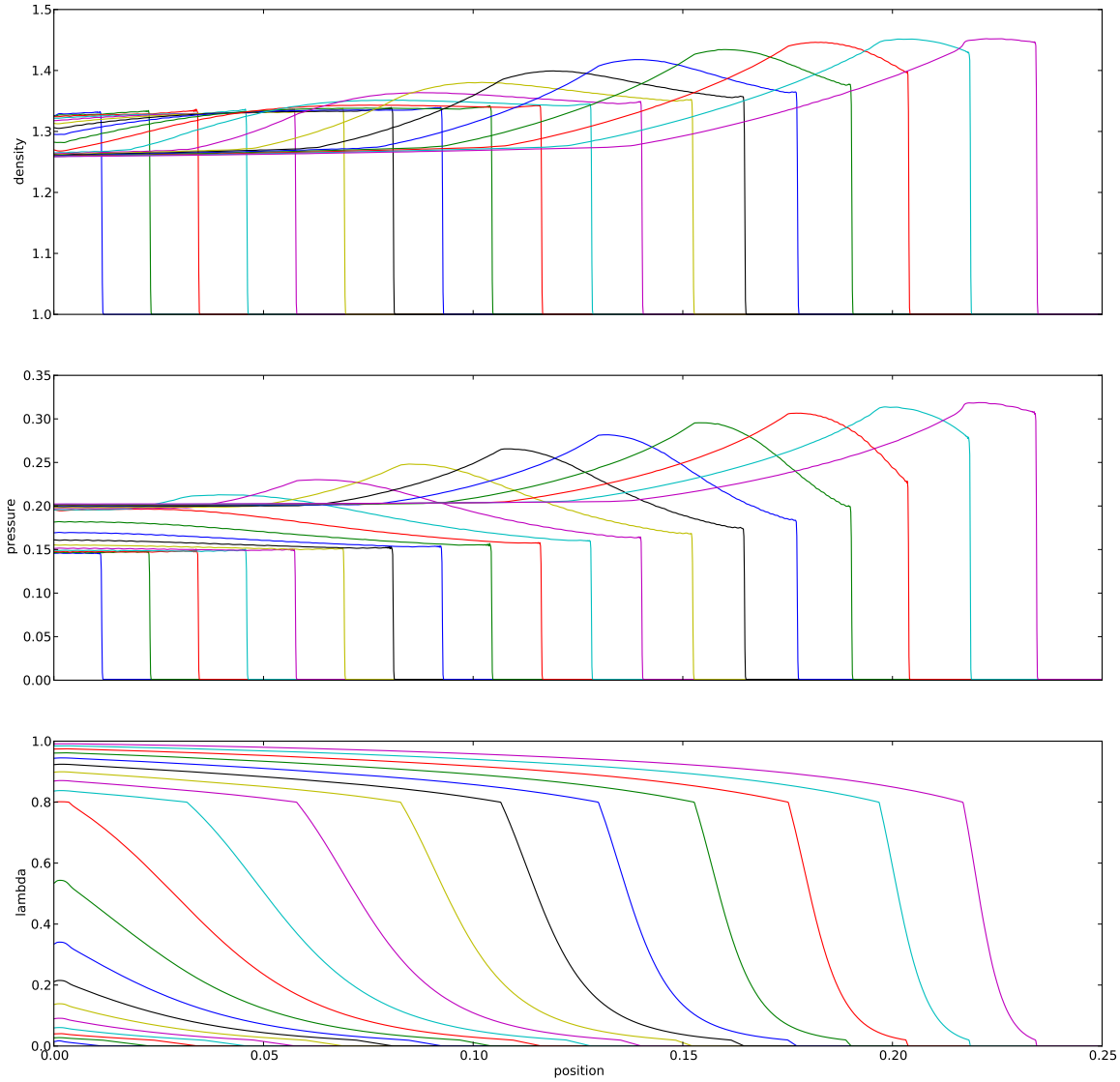

Figure 23: High speed piston impact experiment on LX-17. Results plotted at times from 0.02 to 0.34 in steps of 0.02 to show the ignition stage. The simulation was run in 2000 grid cells (between 0 and 0.25) with temperature equilibrium.

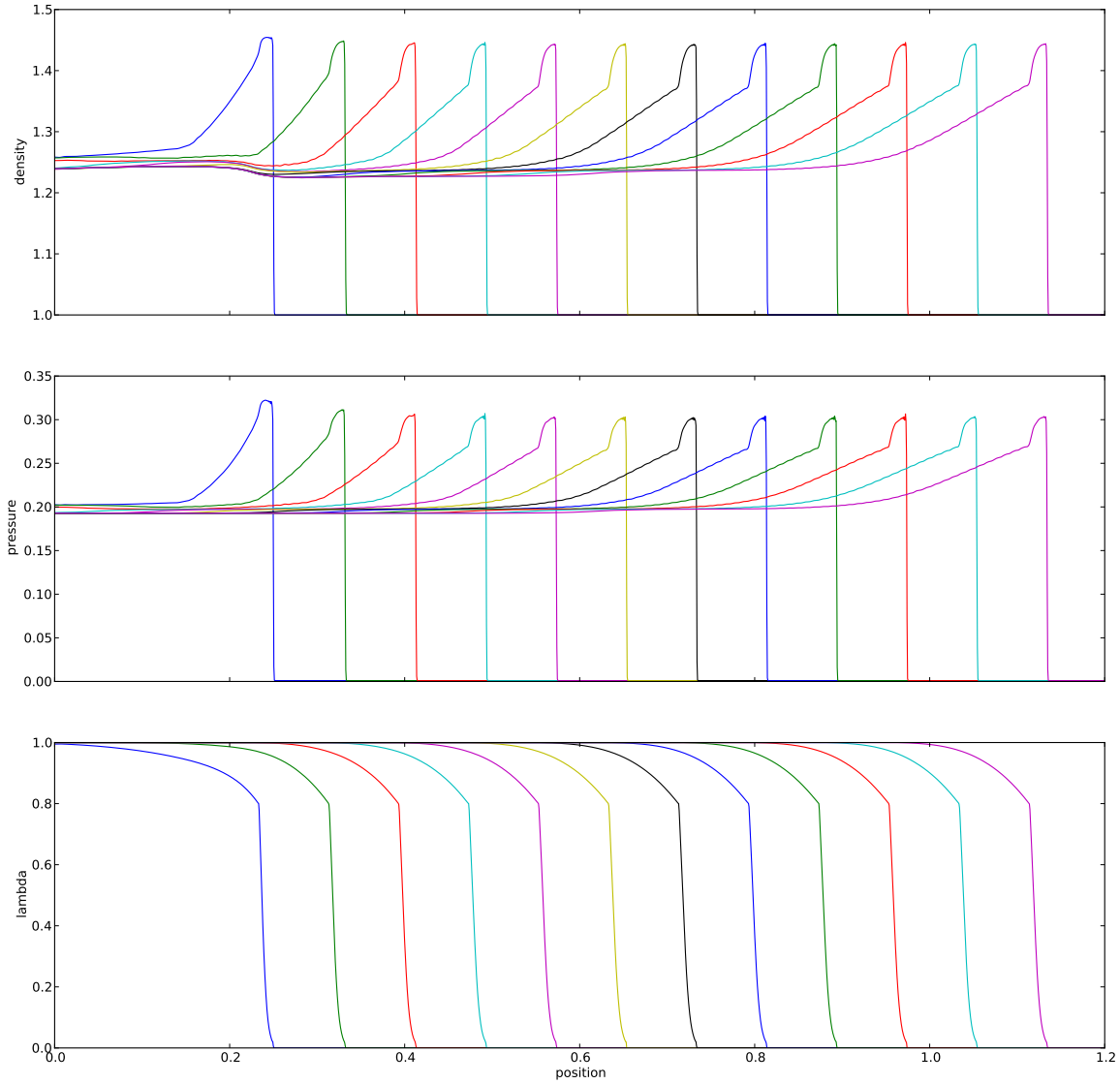

Figure 24: High speed piston impact experiment on LX-17. Results plotted at times from 0.4 to 1.5 in steps of 0.1 to show the steady state stage. The simulation was run in 2000 grid cells (between 0 and 1.2) with temperature equilibrium.

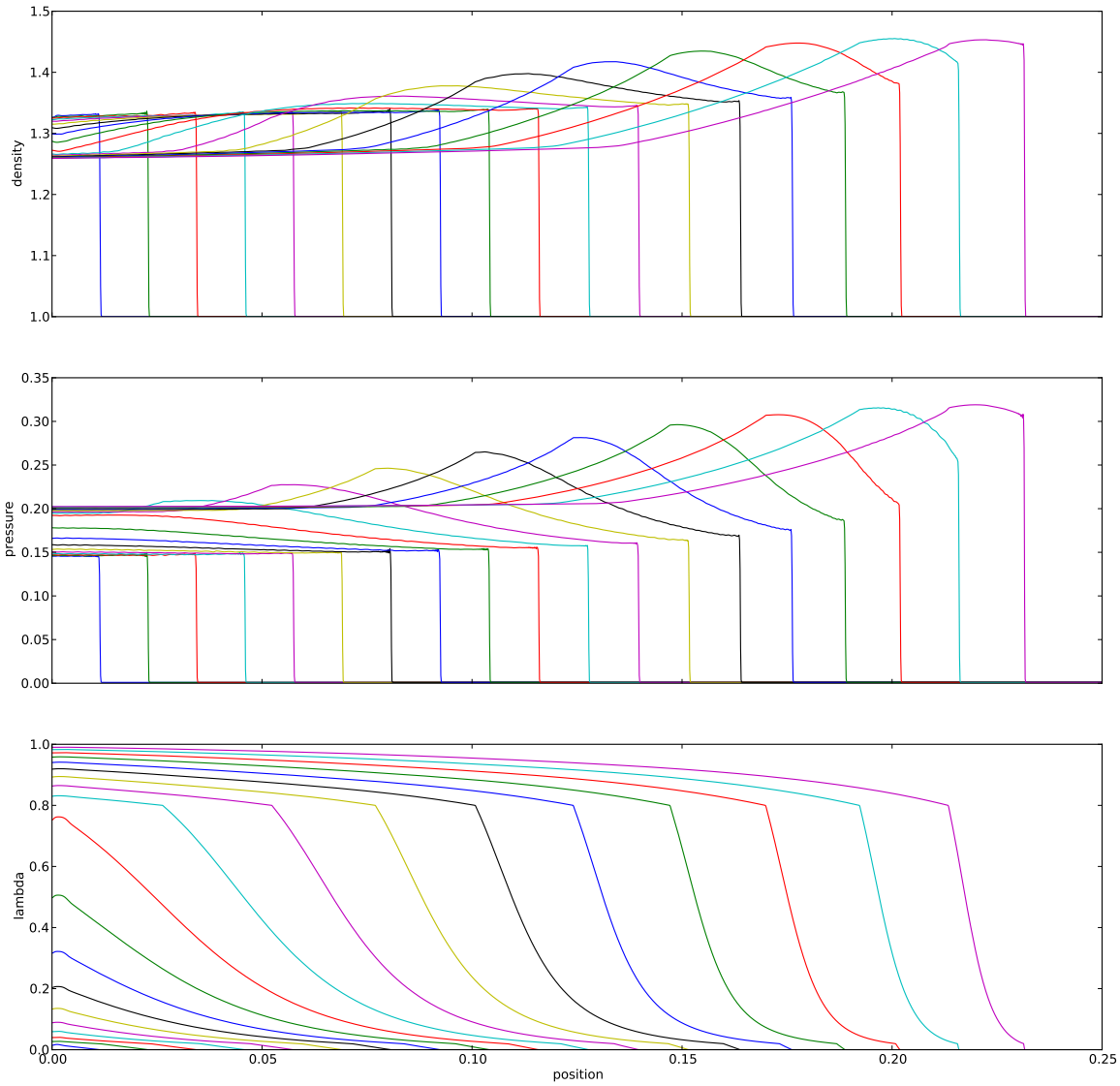

Figure 25: High speed piston impact experiment on LX-17. Results plotted at times from 0.02 to 0.34 in steps of 0.02 to show the ignition stage. The simulation was run in 2000 grid cells (between 0 and 0.25) with the constant volume ratio approximation.

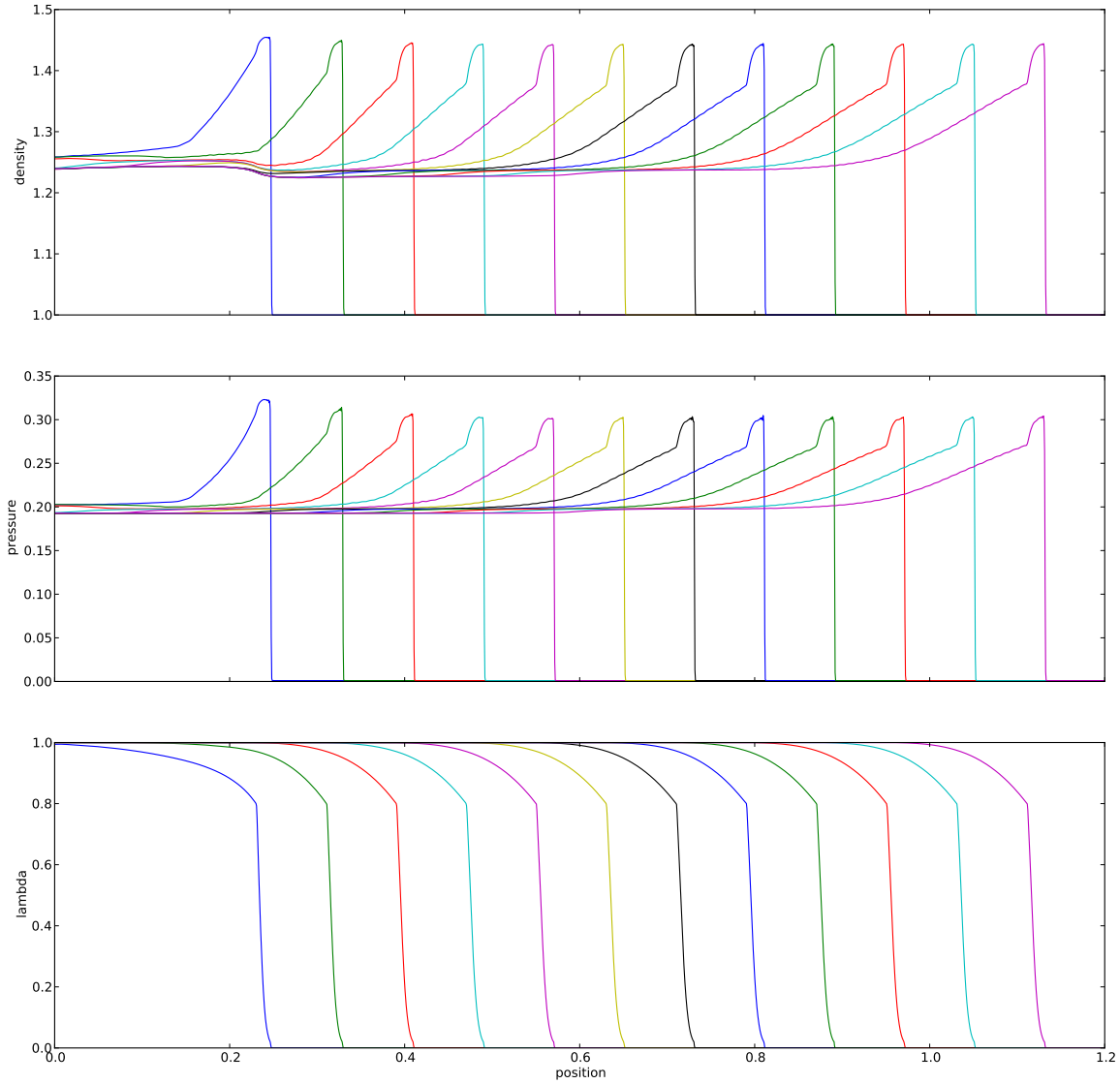

Figure 26: High speed piston impact experiment on LX-17. Results plotted at times from 0.4 to 1.5 in steps of 0.1 to show the steady state stage. The simulation was run in 2000 grid cells (between 0 and 1.2) with constant volume ratio approximation.

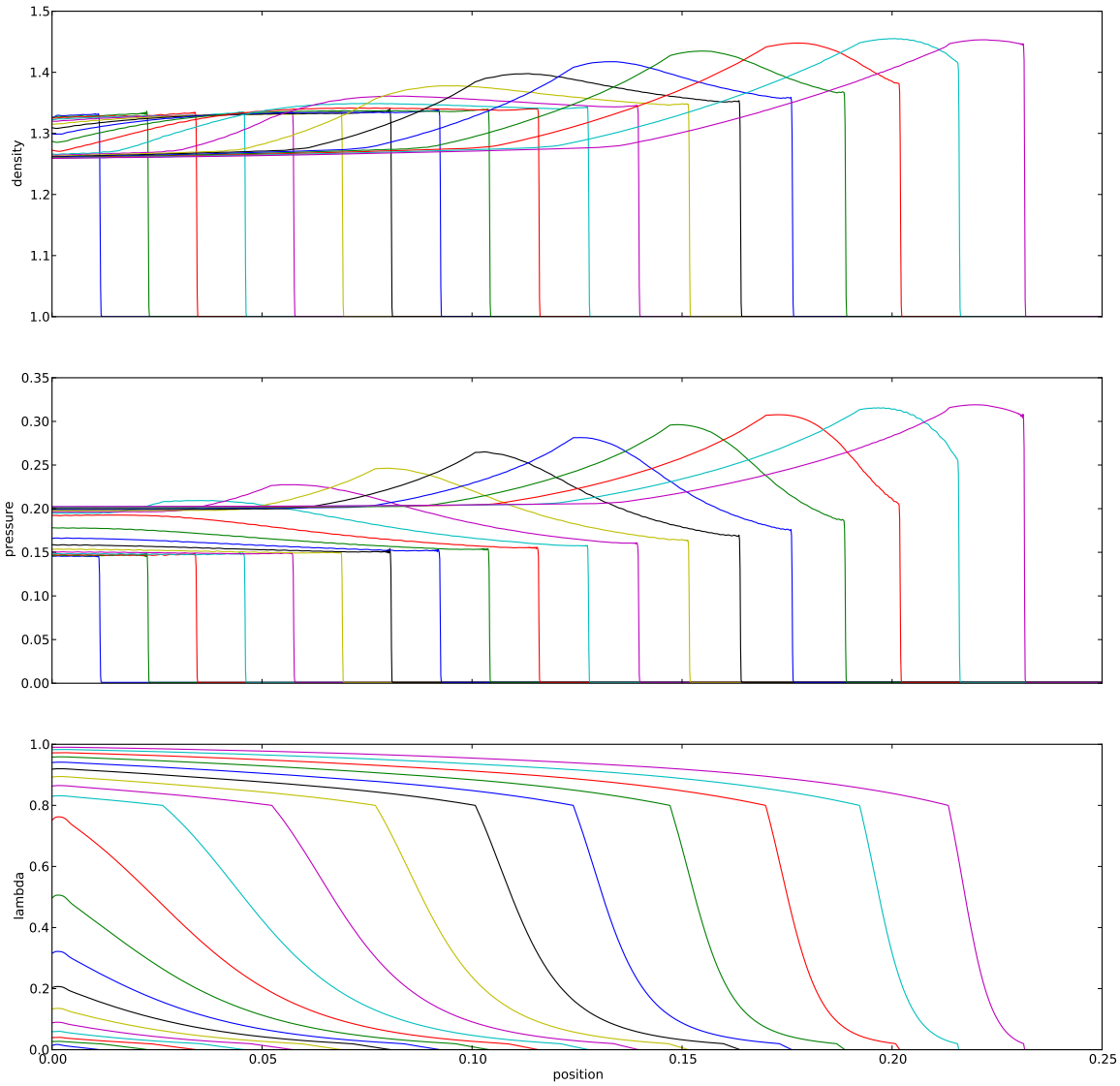

Figure 27: High speed piston impact experiment on LX-17. Results plotted at times from 0.02 to 0.34 in steps of 0.02 to show the ignition stage. The simulation was run in 2000 grid cells (between 0 and 0.25) with isentropic closure (thermal isolation).

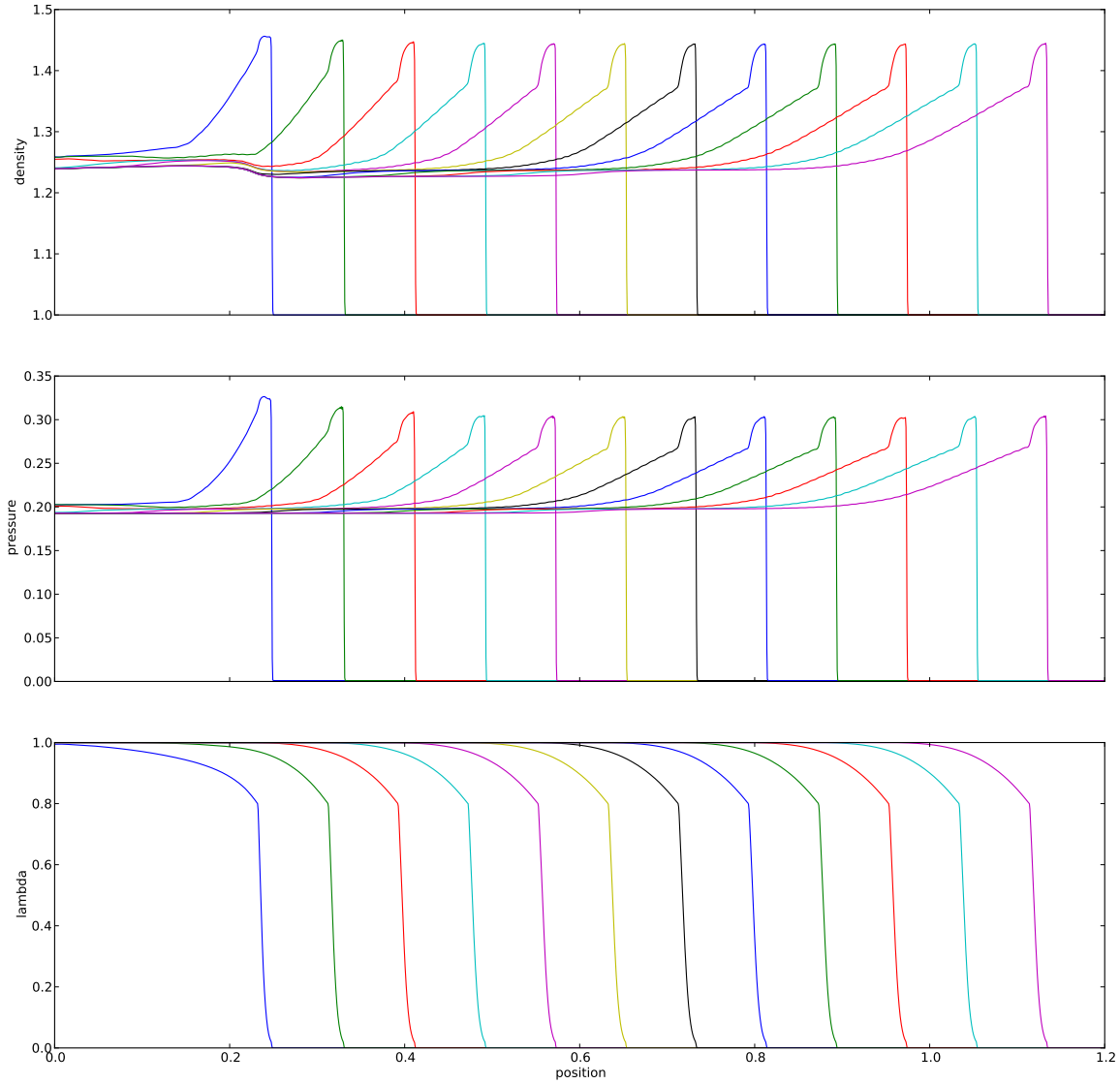

Figure 28: High speed piston impact experiment on LX-17. Results plotted at times from 0.4 to 1.5 in steps of 0.1 to show the steady state stage. The simulation was run in 2000 grid cells (between 0 and 1.2) with isentropic closure (thermal isolation).

5.6. Piston Impact Results with Simplified Reaction Rate

We now consider some very similar experiments to those shown above, but replace the complex ignition and growth reaction rate with a simplified model. This model is not intended to match the results of any particular experiment or material, but will allow a clear comparison between the three closure conditions. The JWL equations of state with the same parameters for LX-17 will be reused from the experiments above. The form of the reaction rate and the parameters used are given in §2.4.

A single test case is considered, with an impact velocity (in scaled units) of 0.13. The results are shown for the three closure conditions in figures 29-31. In these figures, both the ignition stage and the evolution at steady state can be seen.

As above, the time evolution of the results is shown by superposing curves of different colours. The results are shown at times from 0.1 to 0.6 in steps of 0.1, at times from 0.65 to 0.9 in steps of 0.05 and at times from 1.0 to 1.2 in steps of 0.1 (15 curves).

Many of the features observed in the above simulations are also seen here. This is especially so for the high speed test case, as without the strong ignition term in the ignition and growth reaction rate, the explosive will not detonate in a heterogeneous fashion. The detonation wave forms at about $t = 0.8$ and quickly reaches steady state at about $t = 0.9$. The precursor shock moves at a speed of approximately 0.53 and the detonation wave moves at approximately 0.87 in the scaled units.

As before, changing the closure assumption does not have a dramatic effect on the results. The temperature equilibrium results are shown in figure 29, the constant ϕ results in figure 30 and the isentropic results in figure 31. The three sets of results all have waves of the same shape, and in all three, the detonation wave is traveling with the same velocity.

The only difference between the three sets of results is the time at which the detonation wave forms. As before, the isentropic closure condition causes the simulated material to behave more sensitively and so the detonation wave forms earliest. With temperature equilibrium, the material is least sensitive, so the detonation wave takes more time to form. The constant ϕ are results almost indistinguishable from the isentropic closure. The different sensitivity of the material is the result of the amount of energy that is exchanged between the phases. With thermal isolation, all the energy is forced to stay in the reactants, whereas with temperature equilibrium, energy from the reactants is donated from the reactants to the products.

It should be noted that the time taken for the detonation wave to form can be easily tuned by adjusting the reaction rate parameters. If the aim was to match the simulated detonation time to a particular experiment, parameters could be chosen to achieve this, regardless of the particular closure condition used.

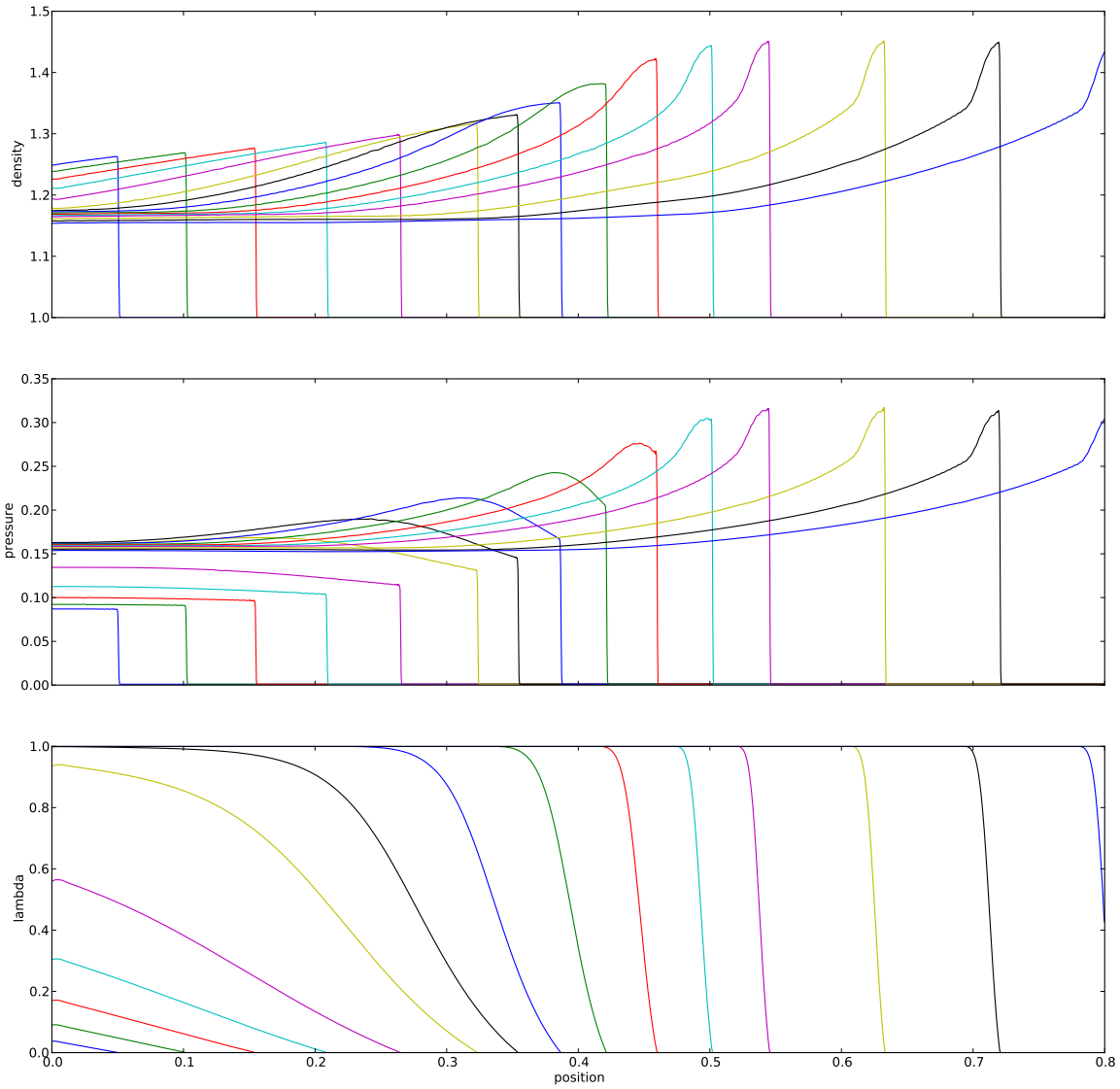

Figure 29: Piston impact experiment on LX-17 with simple reaction rate. Results plotted at times from 0.1 to 0.6 in steps of 0.1, times from 0.65 to 0.9 in steps of 0.05, and 1.0 to 1.2 in steps of 0.1. The simulation was run in 2000 grid cells (between 0 and 0.8) with temperature equilibrium.

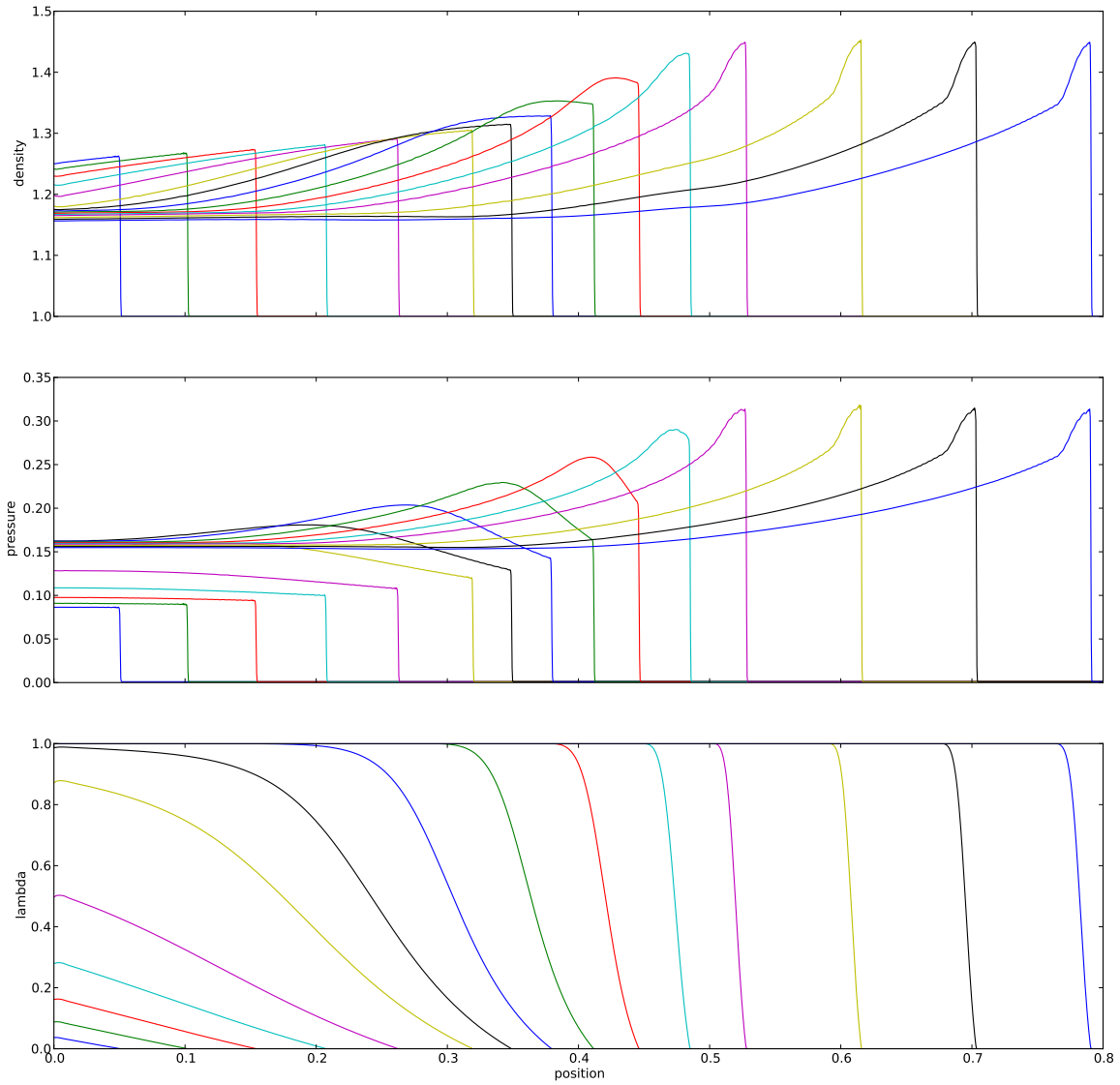

Figure 30: Piston impact experiment on LX-17 with simple reaction rate. Results plotted at times from 0.1 to 0.6 in steps of 0.1, times from 0.65 to 0.9 in steps of 0.05, and 1.0 to 1.2 in steps of 0.1. The simulation was run in 2000 grid cells (between 0 and 0.8) with constant volume ratio approximation.

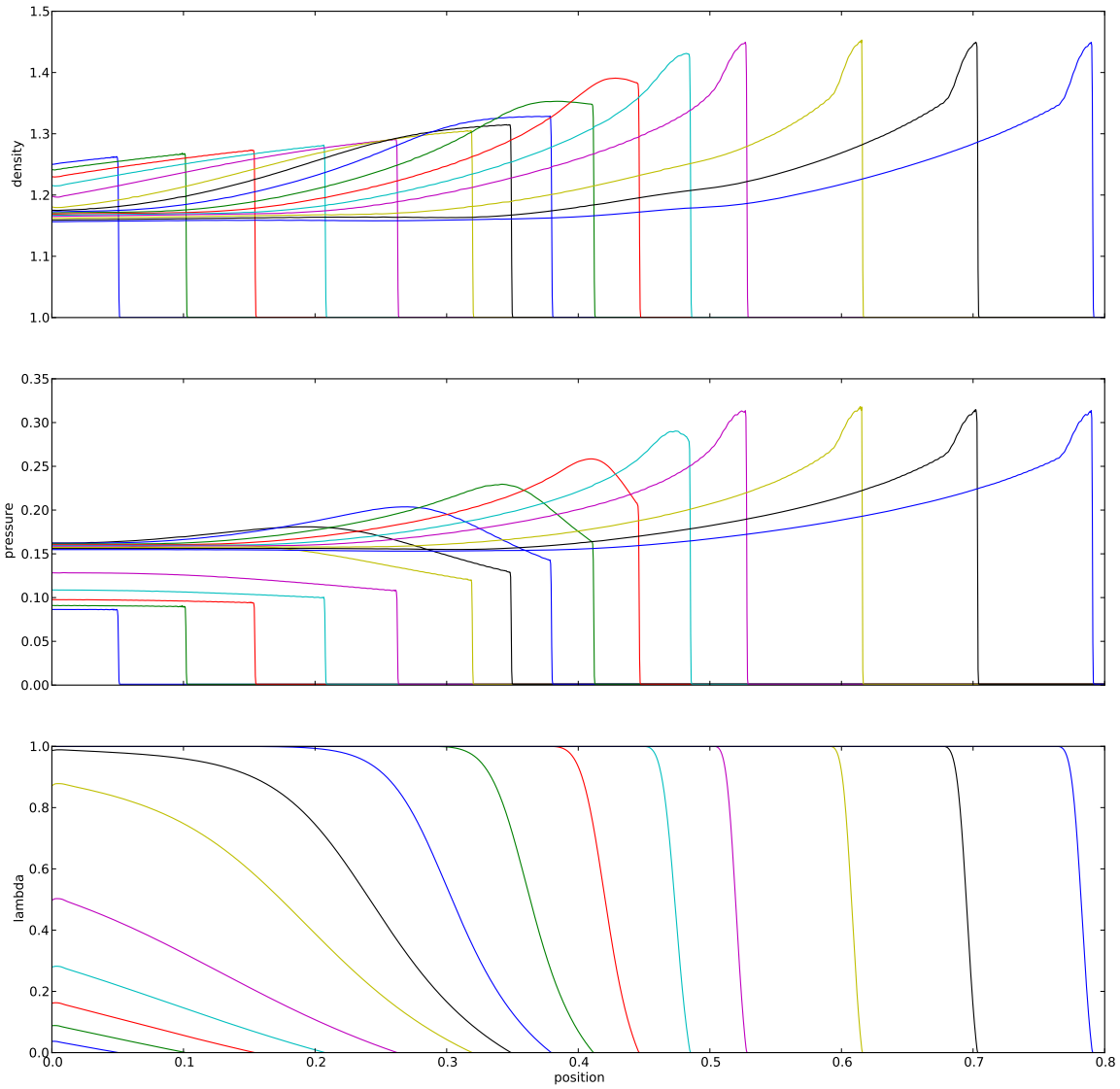

Figure 31: Piston impact experiment on LX-17 with simple reaction rate. Results plotted at times from 0.1 to 0.6 in steps of 0.1, times from 0.65 to 0.9 in steps of 0.05, and 1.0 to 1.2 in steps of 0.1. The simulation was run in 2000 grid cells (between 0 and 0.8) isentropic closure (thermal isolation).

5.7. Discussion

In the experiments performed above, we have compared the effect of applying different closure conditions to form a mixture equation of state.

In the ignition and growth results, applying the constant ϕ and isentropic closure conditions gave results with strange, unphysical features. In particular, the isentropic closure led to the formation of an extra pressure pulse. These strange features can be attributed to the complexity of the ignition and growth reaction rate; the rate law includes so many parameters, all highly tuned to the particular scenario, and so is very sensitive to changes in the model.

Despite the extra features present in the ignition and growth results, it can be seen that applying the isentropic closure condition leads to a sensitisation of the material. To narrow down on this particular aspect, the experiments were repeated with a simplified rate law (defined in §2.4). These experiments reinforced this conclusion.

However, it should be noted that the sensitivity of the material is easily adjusted using the parameters in the reaction rate. This means that the model could be adjusted to give good results, regardless of which closure condition is applied.

While the choice of the closure condition does not have a big impact on the results, it does have a large effect on the computational complexity. In the temperature equilibrium and thermal isolation cases, the mixture equation is defined implicitly, and so requires a iterative root finding procedure. However, the constant ϕ approximation is evaluated explicitly. Typically, the numerical experiments for constant ϕ condition take under half the computer time required for the temperature equilibrium case. Also, in the numerical experiments described here, the majority of cells in the domain are in a pure state with $\lambda = 1$ or 0. In a simulation with more of the cells in a mixed state, the difference in run time would be even more apparent.

As the computationally convenient constant ϕ approximation produces results of the same quality as both the widely used temperature equilibrium closure and the physically motivated thermal isolation, but with much less computational expense, this is a strong contender for extension to simulations in higher dimensions.

6. Conclusions

In this study, numerical solutions of 1-D piston impact problems have been obtained for the evolution from shock induced ignition to steady state detonation of two different high-explosives, Nitromethane (NM) and LX-17.

A numerical solver (hydrocode) for the reactive Euler equations has been developed. This uses a finite volume method to model the flow of the mixture of explosive reactants and products. The code was designed to investigate different methods for forming the equation of state for the mixture: either using a single equation of state to describe the whole mixture or using separate equations for each component material. Furthermore, when building a mixture equation of state by combining individual equations, three different assumptions to close the system could be used. The final element of the solver is the reaction rate law. Most of the simulations were performed using the ignition and growth model, but other reaction rates are easily implemented. The components of hydrocode were validated by comparison with other published results and excellent agreement was obtained.

For NM, the use of a *single* JWL equation of state for the mixture of reactants and products was compared with a *combined* equation of state. In the latter case, the combined equation was derived from two separate JWL equations of state for the reactant and the product phases with a closure condition of temperature equilibrium. These two approaches were compared by performing a shock-induced ignition simulation that mimics the recent experiments of Dattelbaum [11]. Parameters for the equation of state and reaction rate law were taken from Tarver [37], who compares with the results of an earlier experiment [32].

I believe that this is the first time simulation results have been compared with the experiment of Dattelbaum, and this is one of the main contributions of the thesis. The results show that both the single and combined equations of state give good results, but as expected, the best agreement with the experiment is obtained with the combined approach.

For LX-17, a combined equation of state obtained from a pair of JWL equations for reactants and products was investigated with three different closure conditions: (i) temperature equilibrium, (ii) constant volume ratio and (iii) isentropic. For each of the closure conditions two different reaction models (i) ignition and growth and (ii) a simple reaction rate law were tested. It has been found that the three closure conditions produce broadly similar results. The constant volume ratio, which is the cheapest computationally, being as good as the widely used temperature equilibrium or the more complex isentropic condition. The isentropic condition retains energy in the explosive reactants, causing the material to appear to be more sensitive and leading to earlier detonation.

Changing the material model caused some unexpected interactions with the ignition and growth reaction model. A further investigation with the simple reaction law gave a clearer comparison between the three closure conditions - again suggesting that the constant volume ratio closure condition is a good candidate for extension to more complex situations.

Note that although others (in particular Stewart [34]) have concentrated on comparisons for the final steady state of the process, we have also presented a comparison of the closure conditions for the full evolution from ignition to steady state detonation.

Further work

In §5.7, we noted that the sensitivity of the material is easily adjusted through the parameters of the reaction rate. The next step in comparing the effects of the three closure conditions would be to attempt to tune these parameters, to confirm that the reactive mixture model gives accurate results regardless of the closure condition applied. This would verify that the more computationally efficient constant volume ratio approximation can be used in future simulations.

This is important as evaluating a complex mixture equation is often the most computationally demanding part of the numerical solution. Whilst computer time is not a limiting factor in one-dimensional simulations, in two- and especially three- dimensional solutions, applying the more efficient closure condition would allow simulations to be performed at higher resolutions.

This will be vital in the next stage of the project, which aims to apply a more axiomatic approach to modelling the formation and growth of hotspots in plastic bonded explosives. The two-phase mixture model with a single (mixture of) reactant(s) and single (mixture of) product(s) will be extended to explicitly include the inert bonding material and its product. Thus, there will be four phases: the solid reactant and bonding material, and the two corresponding gaseous states of the products. Two dimensional scenarios much like those presented by Handley [18] will be considered.

For this future requirement, some of the assumptions made in this work are not valid. In particular, the empirical ignition and growth reaction rate will be replaced with an Arrhenius chemistry model, and the diffusion terms of the Navier-Stokes equations will be included to represent the effects of turbulence. This may require more sophisticated solution methods, as in the work of Don et al. [12, 13, 16].

A. Code Verification

A.1. Shock Tube Problems

Toro [38] defines four useful problems for testing the inert part of the solver. These are designed to exercise a solver for all possible wave patterns in the Euler equations.

These tests are in the form of *shock-tube* problems. A shock tube is a one dimensional, idealised representation of an experimental setup. The initial data gives two states $(\rho, u, p)_{\mathrm{L}}$ and $(\rho, u, p)_{\mathrm{R}}$ which fill the two ends of the tube. These states are separated by a thin membrane at position m_0. This setup is illustrated in figure 32.

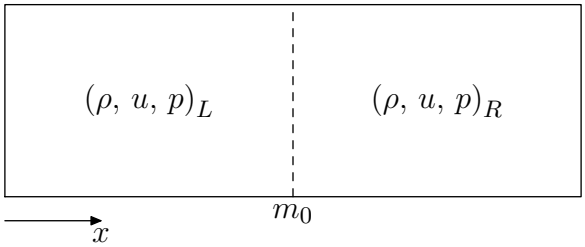

Figure 32: Sketch of a shock tube problem.

At time $t = 0$, the membrane is removed and the simulation is started. These problems are useful tests, as the exact solution is fairly easily generated by solving the Riemann problem. In the results shown here, exact solutions were generated using code from Toro's NUMERICA package [38].

In table 6, the four test problems are defined. The initial conditions are given, along with the membrane position m_0 and the simulation end time $t_{\max}$. The parameters are given in arbitrary scaled units.

My results of the four tests are shown in figures 33-36. Tests 1 and 2 were run with 200 cells and tests 3 and 4 were run with 400 cells. The results shown that even at this low resolution, the SLIC method with the VANLEER limiter performs well, except for the particularly difficult test case in figure 34. An excellent agreement is found between these results and those shown by Toro [38, §14.7].

Test	ρ_{L}	u_{L}	p_{L}	ρ_{R}	u_{R}	p_{R}	m_0	$t_{\max}$
1	1.0	0.75	1.0	0.125	0.0	0.1	0.3	0.25
2	1.0	-2.0	0.4	1.0	2.0	0.4	0.5	0.15
3	1.0	0.0	1000.0	1.0	0.0	0.01	0.5	0.012
4	5.99924	19.5975	460.894	5.99242	-6.19633	46.0950	0.4	0.035

Table 6: The 4 test cases defined by Toro [38]. These are in scaled units.

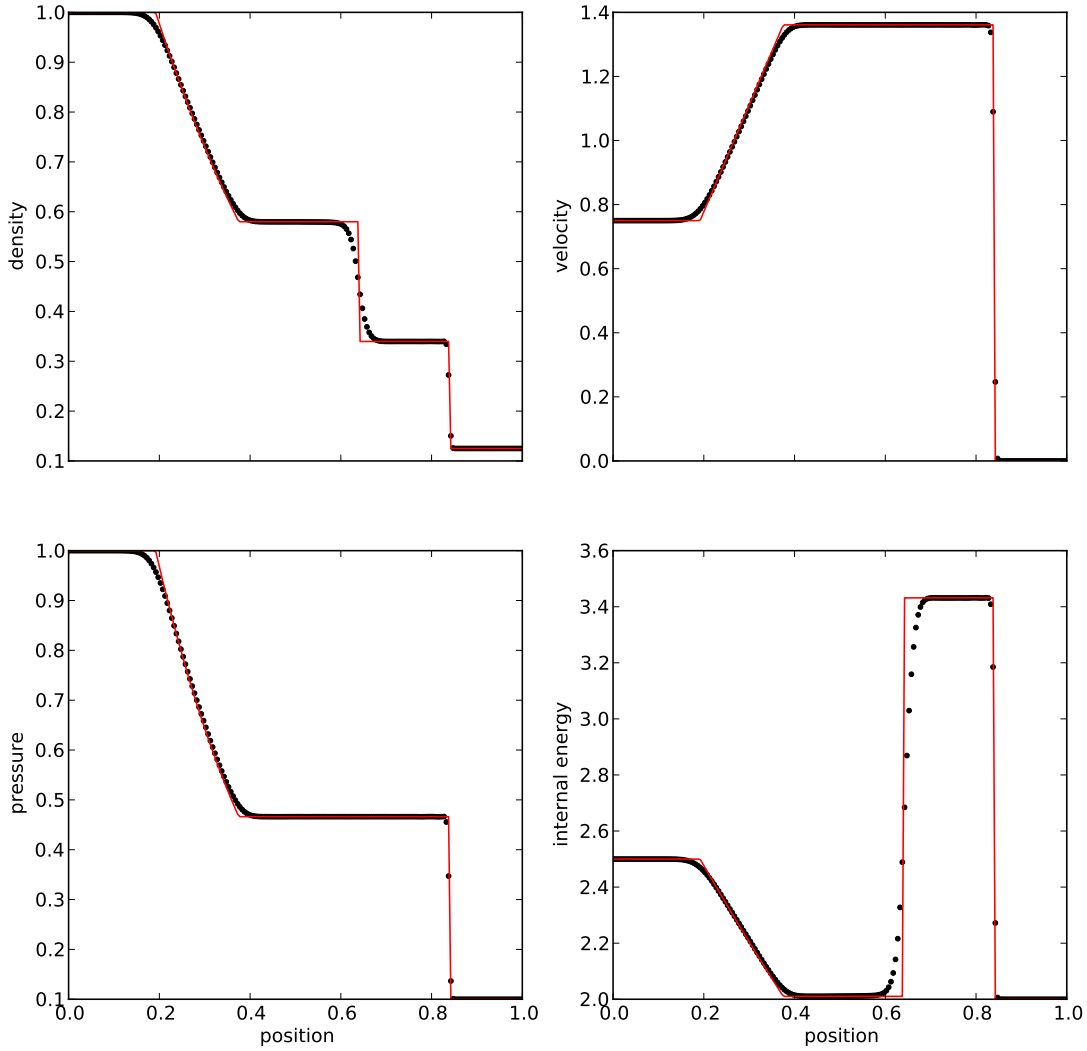

Figure 33: Toro's 1st test. Numerical solution (black points) calculated in 200 cells using the SLIC method with the VANLEER limiter plotted with the exact solution (red line).

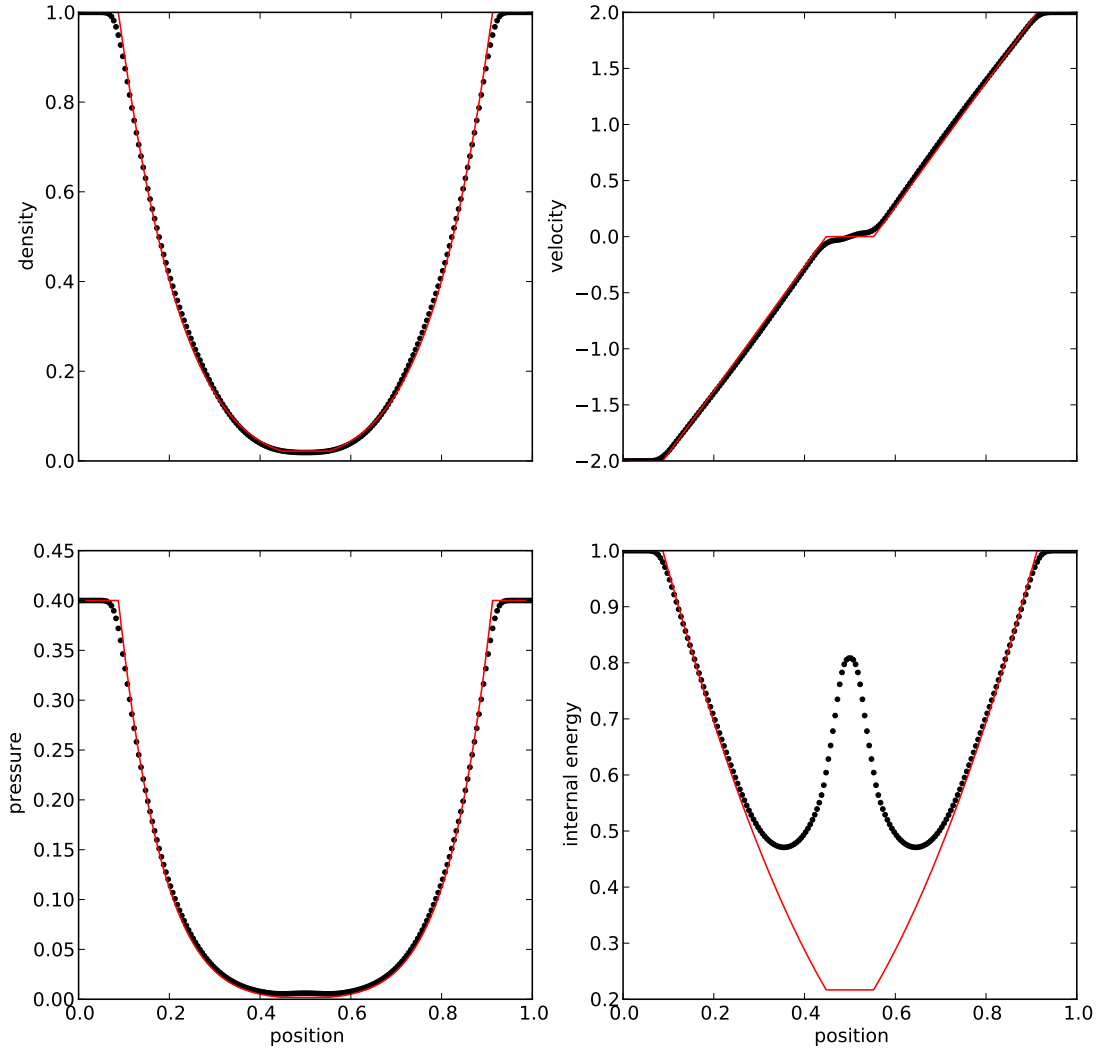

Figure 34: Toro's 2nd test. Numerical solution (black points) calculated in 200 cells using the SLIC method with the VANLEER limiter plotted with the exact solution (red line).

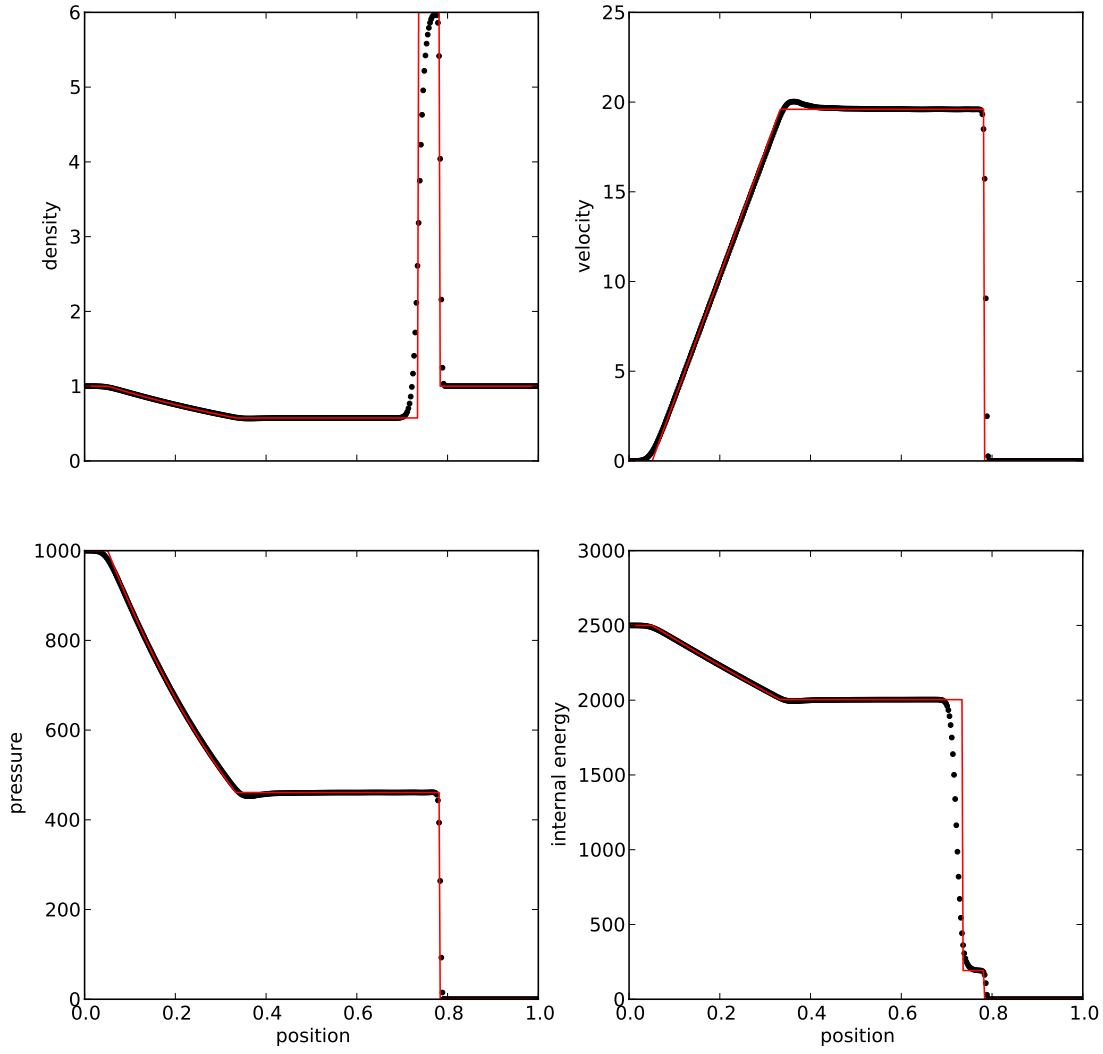

Figure 35: Toro's 3nd test. Numerical solution (black points) calculated in 400 cells using the SLIC method with the VANLEER limiter plotted with the exact solution (red line).

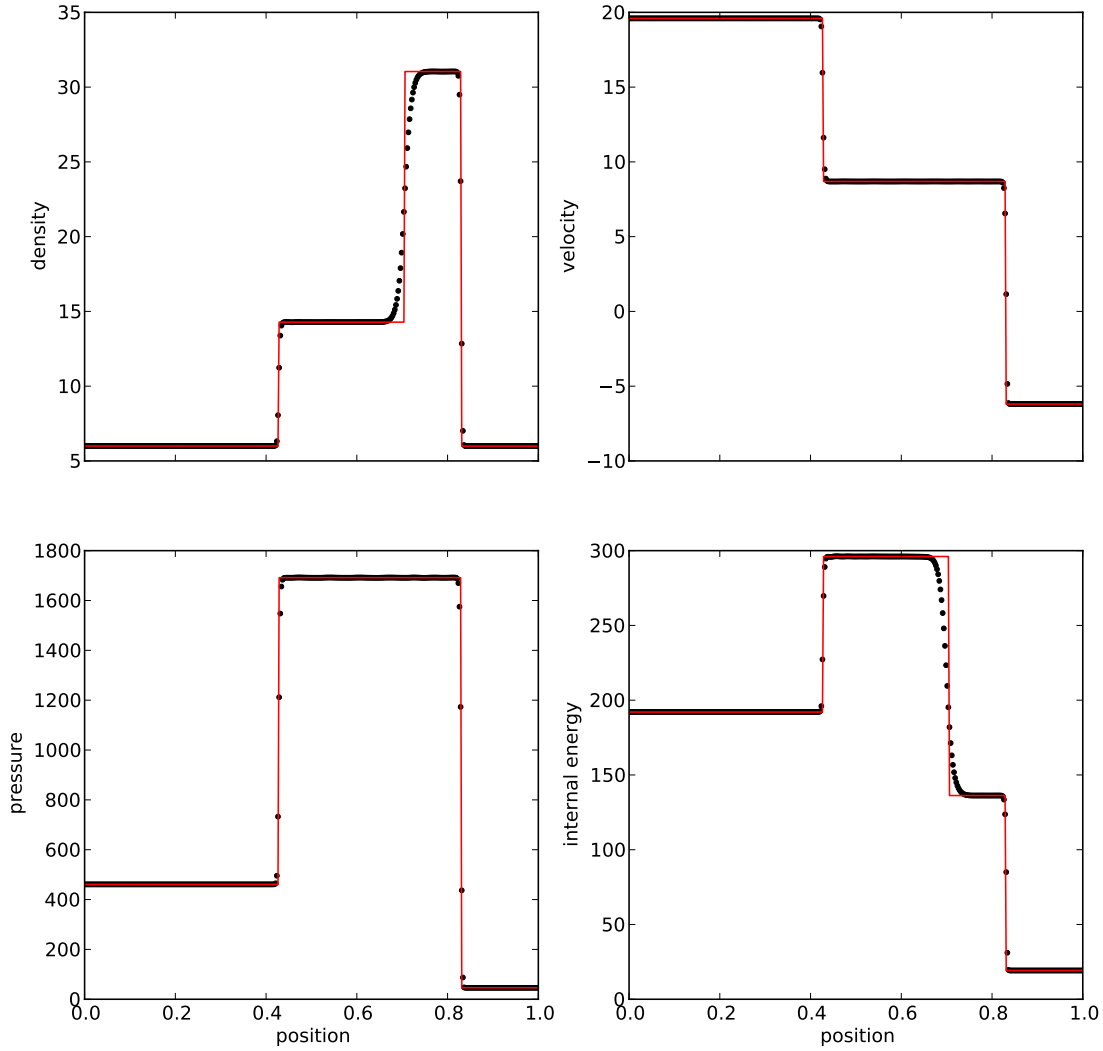

Figure 36: Toro's 4th test. Numerical solution (black points) calculated in 400 cells using the SLIC method with the VANLEER limiter plotted with the exact solution (red line).

A.2. Comparison to Kapila et al.

In section 5.4, the results of piston impact simulations on LX-17 were presented. These simulations were based on test cases defined in a paper of Kapila et al. [20], and so some of the results in §5.4 can be directly compared with Kapila's results.

The simulations performed here use the same scaling as Kapila, so the results are directly comparable. This allows for a quantitative comparison of some particular values from the simulation and a qualitative comparison of the results at the end of a full hyperbolic evolution.

By solving for the intersection between the Rayleigh line and the Hugoniot of the reactants, we can find the von Neumann state. Similarly, finding the point where the Rayleigh line meets the product Hugoniot gives the Chapman-Jouguet state. The values of pressure and specific volume at these states as found by Kapila and me are given in table 7.

	Kapila [20]		My results	
	pressure	volume	pressure	volume
CJ	0.24029737	0.75970263	0.24097	0.76003
VN	0.30992878	0.69007122	0.31056	0.69044

Table 7: Comparison with Kapila [20, p.11] of calculated pressures and specific volumes at the Chapman-Jouguet (CJ) and von Neumann (VN) states.

The values in table 7 show excellent agreement. The discrepancy of less than 1% is thought to be due to numerical errors and different methods of solution.

These values test the correctness of the implementation of the equation of state. To verify that the reaction rate law was being calculated correctly, the plot of the reaction rate in figure 4 was compared with the similar plot from Kapila [20, Fig. 1(c)].

In order to test the implementation of the hydrocode as a whole, Kapila's test cases were repeated. The low and high speed piston impact tests, as described and discussed in §5.4, are both plotted in the early ignition stage and at the late stage when the solution has reached steady state. My solutions are compared to those from Kapila [20] in figures 37-40. Again, there is excellent agreement, and the solutions are almost indistinguishable to the eye.

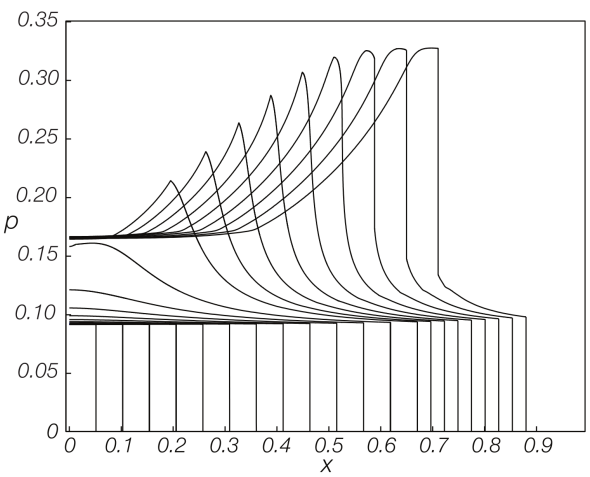

(a) Results from Kapila [20].

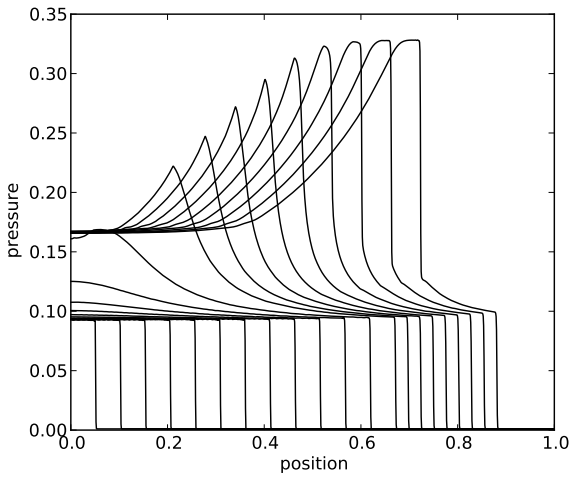

(b) This work.

Figure 37: Comparison of ignition stage results for the low speed impact test case.

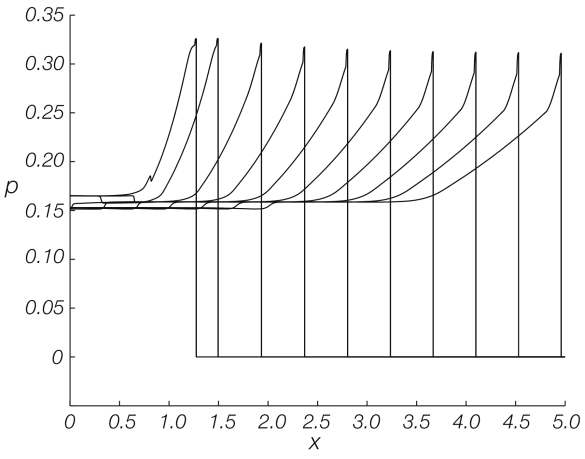

(a) Results from Kapila [20].

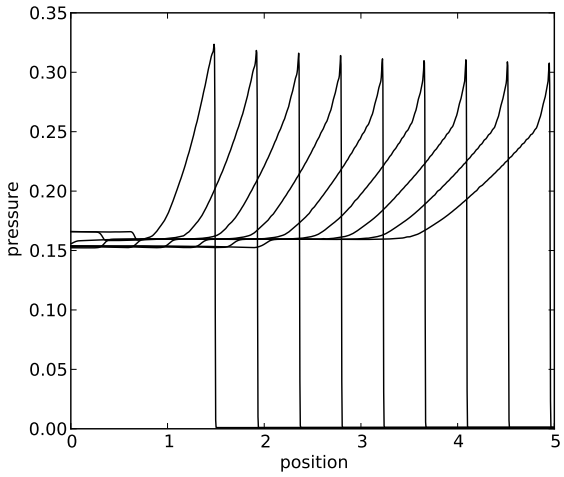

(b) This work.

Figure 38: Comparison of steady-state stage results for the low speed impact test case.

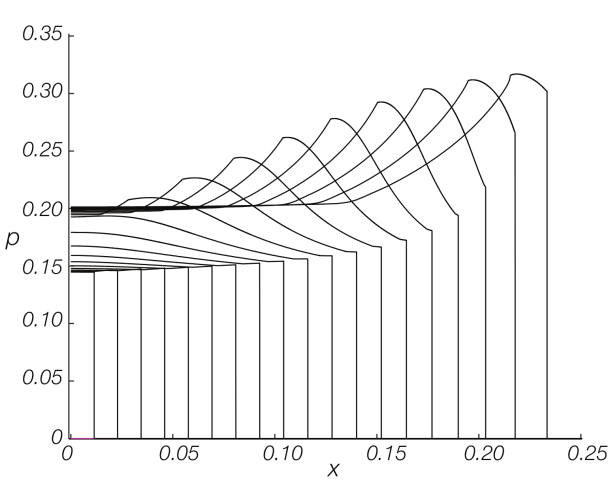

(a) Results from Kapila [20].

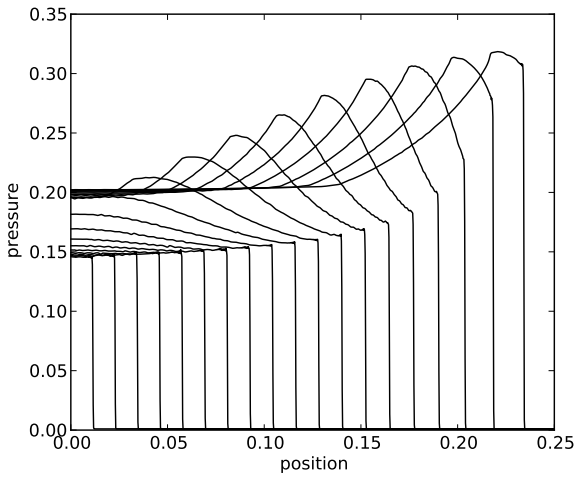

(b) This work.

Figure 39: Comparison of ignition stage results for the high speed impact test case.

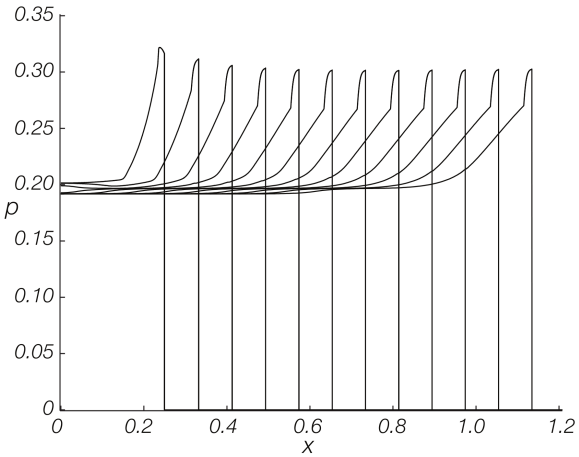

(a) Results from Kapila [20].

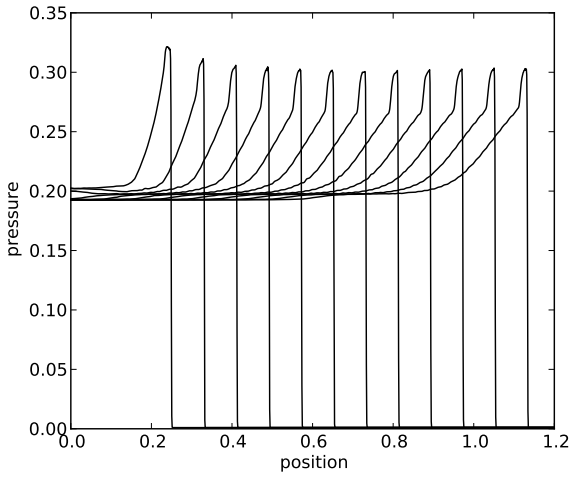

(b) This work.

Figure 40: Comparison of steady-state stage results for the high speed impact test case.

References

[1] Allaire, G., Clerc, S., and Kokh, S. A Five-Equation Model for the Simulation of Interfaces between Compressible Fluids. *Journal of Computational Physics 181*, 2 (Sept. 2002), 577–616.

[2] Baer, M., and Nunziato, J. A two-phase mixture theory for the deflagration-to-detonation transition (DDT) in reactive granular materials. *International journal of multiphase flow 12*, 6 (Nov. 1986), 861–889.

[3] Banks, J., Henshaw, W., Schwendeman, D., and Kapila, A. A study of detonation propagation and diffraction with compliant confinement. *Theory and Modelling* (2008), 1–37.

[4] Barlow, A. *An Adaptive Multi-Material Arbitrary Lagrangian Eulerian Algorithm for Computational Shock Hydrodynamics*. PhD thesis, Swansea, 2002.

[5] Bdzil, J., Menikoff, R., Son, S., Kapila, A., and Stewart, D. S. Two-phase modeling of deflagration-to-detonation transition in granular materials: A critical examination of modeling issues. *Physics of Fluids 11*, 2 (1999), 378.

[6] Brown, W. B., Feng, Z., and Braithwaite, M. Williamsburg equation of state for modelling non-ideal detonation. *Le Journal de Physique IV 5* (1995).

[7] Campbell, A., Davis, W. C., Ramsay, J., and Travis, J. Shock Initiation of Solid Explosives. *Physics of Fluids 4*, 4 (1961), 511.

[8] Campbell, A., Davis, W. C., and Travis, J. Shock Initiation of Detonation in Liquid Explosives. *Physics of Fluids 4*, 4 (1961), 498.

[9] Chinnayya, A., Daniel, E., and Saurel, R. Modelling detonation waves in heterogeneous energetic materials. *Journal of Computational Physics 196*, 2 (May 2004), 490–538.

[10] Courant, R., Friedrichs, K., and Lewy, H. Über die partiellen Differenzengleichungen der mathematischen Physik. *Mathematische Annalen 100*, 1 (1928), 32–74.

[11] Dattelbaum, D., Sheffield, S., Stahl, D., Dattelbaum, A., Trott, W., and Engelke, R. Influence of hot spot features on the initiation characteristics of heterogeneous nitromethane. In *International Detonation Symposium* (2010), vol. 836.

[12] Don, W. S. Numerical Study of Pseudospectral Methods in Shock Wave Applications. *Journal of Computational Physics 110*, 1 (1994), 103–111.

[13] Don, W. S., and Quillen, C. B. Numerical Simulation of Shock-Cylinder Interactions. *Journal of Computational Physics 122* (1995), 244–265.

[14] Dunnett, J., Swift, D., and Braithwaite, M. Comparison of Williamsburg and JWL equations of state for nitromethane. *Eleventh International Detonation* (2008).

[15] Fickett, W., and Davis, W. C. *Detonation: Theory and Experiment*. Dover, 2000.

[16] Gottlieb, D., and Don, W. S. Spectral simulation of supersonic reactive flows. *SIAM journal on numerical analysis 35*, 6 (1998), 2370–2384.

[17] Gustavsen, R., Sheffield, S., Alcon, R., Forbes, J., Tarver, C. M., and Garcia, F. Embedded Electromagnetic Gauge Measurements and Modeling of Shock Initiation in the TATB Based Explosives LX-17 and PBX 9502. In *AIP Conference Proceedings* (2002), pp. 1019–1022.

[18] Handley, C. A. *Numerical modelling of two HMX-based plastic-bonded explosives at the mesoscale*. PhD thesis, St Andrews, 2011.

[19] Kapila, A., Menikoff, R., Bdzil, J., Son, S., and Stewart, D. S. Two-phase modeling of deflagration-to-detonation transition in granular materials: Reduced equations. *Physics of Fluids 13*, 10 (2001), 3002.

[20] Kapila, A., Schwendeman, D., and Bdzil, J. A study of detonation diffraction in the ignition-and-growth model. *Combustion Theory and Modelling* (2007), 1–41.

[21] Lee, E., Horning, H., and Kury, J. Adiabatic expansion of high explosive detonation products. Tech. rep., Lawrence Radiation Laboratory, 1968.

[22] Lee, E., and Tarver, C. M. Phenomenological model of shock initiation in heterogeneous explosives. *Physics of Fluids 23*, 12 (1980), 2362.

[23] LeVeque, R. *Finite volume methods for hyperbolic problems*. Cambridge University Press, 2007.

[24] Menikoff, R., and Shaw, M. Reactive burn models and ignition & growth concept. *EPJ Web of Conferences 10* (Jan. 2011), 00003.

[25] Nichols, A. L., and Tarver, C. M. A Statistical Hot Spot Reactive Flow Model for Shock Initiation and Detonation of Solid High Explosives. In *12th International Detonation Symposium, San Diego, CA* (2002).

[26] Petitpas, F., Franquet, E., Saurel, R., and Le Metayer, O. A relaxation-projection method for compressible flows. Part II: Artificial heat exchanges for multiphase shocks. *Journal of Computational Physics 225*, 2 (Aug. 2007), 2214–2248.

[27] Petitpas, F., Saurel, R., Franquet, E., and Chinnayya, A. Modelling detonation waves in condensed energetic materials: multiphase CJ conditions and multidimensional computations. *Shock waves 19*, 5 (2009), 377–401.

[28] Radhakrishnan, K., and Hindmarsh, A. C. Description and Use of LSODE , the Livermore Solver for Ordinary Differential Equations. Tech. rep., Lawrence Livermore National Laboratory, 1993.

[29] Saurel, R., Franquet, E., Daniel, E., and Le Metayer, O. A relaxation-projection method for compressible flows. Part I: The numerical equation of state for the Euler equations. *Journal of Computational Physics 223*, 2 (May 2007), 822–845.

[30] Schwendeman, D., and Kapila, A. A study of detonation diffraction and failure for a model of compressible two-phase reactive flow. *Combustion Theory and Modelling* (2010), 1–33.

[31] Schwendeman, D., Kapila, A., and Henshaw, W. A Comparative Study of Two Macro-Scale Models of Condensed-Phase Explosives. *IMA Journal of Applied Mathematics 1* (2005), 17.

[32] Sheffield, S., Engelke, R., Alcon, R., Gustavsen, R. L., Robbins, D. L., Stahl, D. B., Stacy, H. L., and Whitehead, M. C. Particle velocity measurements of the reaction zone in nitromethane. In *12th International Detonation Symposium, San Diego, CA* (2002), vol. 836, pp. 0–8.

[33] Stewart, D. S., Asay, B. W., and Prasad, K. Simplified modeling of transition to detonation in porous energetic materials. *Physics of Fluids 6*, 7 (1994), 2515.

[34] Stewart, D. S., and Yoo, S. Equation of state for modeling the detonation reaction zone. *12th Symp.(Intl) on Detonation* (2002).

[35] Tarver, C. M. Reactive flow modeling of the interaction of TATB detonation waves with inert materials. *Twelfth International Detonation*, 1 (2002), 1–10.

[36] Tarver, C. M. Ignition and Growth Modeling of LX-17 Hockey Puck Experiments. *Propellants, Explosives, Pyrotechnics 30*, 2 (Apr. 2005), 109–117.

[37] Tarver, C. M., and Urtiew, P. A. Theory and Modeling of Liquid Explosive Detonation. *Journal of Energetic Materials 28*, 4 (Oct. 2010), 299–317.

[38] Toro, E. F. *Riemann solvers and numerical methods for fluid dynamics*. Springer, 2009.

[39] Whitworth, N. *Mathematical and Numerical Modelling of Shock Initiation in Heterogeneous Solid Explosives*. PhD thesis, Cranfield University, 2008.